In presenting this dissertation/thesis as a partial fulfillment of the requirements for an advanced degree from Emory University, I agree that the Library of the University shall make it available for inspection and circulation in accordance with its regulations governing materials of this type. I agree that permission to copy from, or to publish, this thesis/dissertation may be granted by the professor under whose direction it was written when such copying or publication is solely for scholarly purposes and does not involve potential financial gain. In the absence of the professor, the dean of the Graduate School may grant permission. It is understood that any copying from, or publication of, this thesis/dissertation which involves potential financial gain will not be allowed without written permission.

Zhe Zhang

Photoinduced Electron Transfer (ET) Dynamics between Molecular Adsorbates and Semiconductor Nanoparticles with Insulating Metal Oxide Overlayers

By
Zhe Zhang
Department of Chemistry

_____

Tianquan Lian, Ph.D.
Advisor

_____

James T. Kindt, Ph.D.
Committee Member

_____

Michael C. Heaven, Ph.D.
Committee Member

Accepted:

_____

Dean of the Graduate School

_____

Date

Photoinduced Electron Transfer (ET) Dynamics between Molecular Adsorbates and Semiconductor Nanoparticles with Insulating Metal Oxide Overlayers

By

Zhe Zhang

B.S Harbin Institute of Technology, P. R. China, 2003

M.S. Shanghai Jiao Tong University, P. R. China, 2006

Advisor: Tianquan Lian, Ph.D.

An Abstract of

A thesis submitted to the Faculty of the Graduate School of Emory University in partial fulfillment of the requirements for the degree of Master of Science

Department of Chemistry

2008

Abstract

Photoinduced interfacial electron transfer (ET) dynamics between adsorbate materials and mesoporous semiconductor nanoparticles could be investigated with ultrafast infrared and visible spectroscopy. Dependence of ET on insulating metal oxide overlayer and interfacial ET between Quantum Dots and Semiconductor has been studied in this work by choosing appropriate dyes and semiconductor nanoparticles.

The dependence of ET dynamics on the number of Al_2O_3 and TiO_2 insulating overlayers has been studied with ultrafast transient spectroscopy. The system of RhB-Al_2O_3-SnO_2 was chosen because ET dynamics for the RhB-SnO_2 system was expected to be relatively fast enough to be completed within 1ns detection time window, thereby facilitating our comparison among injection dynamics. Injection yield was shown to decrease with the increase of the number of Al_2O_3 overlayers. Electron injection dynamics was shown to be slowed down as the number of Al_2O_3 overlayers increases in both transient infrared and visible experiment. For the RuN3-TiO_2-SnO_2 and C343-TiO_2-SnO_2 systems, the injection yields decrease with the increase of number of TiO_2 overlayers from zero to two. However, the injection yields for that with 3 three overlayers is always larger. Detail is still to be understood.

ET dynamics from TOPO capped CdSe QDs to TiO_2 nanoparticles were also monitored with ultrafast transient spectroscopy. No electron transfer was observed from the analysis of both transient mid-IR and transient visible experiments. Thiol and dithiocarbamate capped CdSe QDs were successfully prepared in an effort for the following preparing TiO_2-CdSe nanocomposite. However, unfortunately, the ligand exchanged QDs were not favorable because of the photostability problem and insufficient absorption onto TiO_2.

Photoinduced Electron Transfer (ET) Dynamics between Molecular Adsorbates and Semiconductor Nanoparticles with Insulating Metal Oxide Overlayers

By

Zhe Zhang

B.S Harbin Institute of Technology, P. R. China, 2003

M.S. Shanghai Jiao Tong University, P. R. China, 2006

Advisor: Tianquan Lian, Ph.D.

An Abstract of

A thesis submitted to the Faculty of the Graduate School of Emory University in partial fulfillment of the requirements for the degree of Master of Science

Department of Chemistry

2008

Tables of Contents

List of Figures

Chapter 1

Chapter 2

Chapter 3

Chapter 4

Chapter 1 Introduction

1.1 General Introduction

As a potential alternative energy resource, solar energy has received extensive attention around the world after the energy crisis in 1970s [1]. Solar cell, a photovoltaic device to convert solar energy to electricity, has become the focus of research interest regarding the utilization of solar energy. Typical conventional solar cell is composed of large area p-n junctions where the photo-generated electrons and holes are swept down the energy barrier by the build-in electric field after diffusing to the junction, therefore producing a forward voltage across the illuminated junction, which is opposite to the built-in field. Even though no exhaust of green-house gas and nuclear waste byproducts when performing the solar-to-electric power conversion, the consideration for the cost-effectiveness still drives people to develop new type of solar cells expecting to possess high efficiency and low cost. Dye sensitized solar cell [2, 3] (DSSC) with the new type of charge separation mechanism is taken as a potential candidate for the next generation solar cell. Compared with conventional p-n junction solar cell, DSSC replace the bulk semiconductor with mesoporous structures with high surface-area, which provides a great enhancement for the dye absorbing. Moreover, charge injection efficiency could be greatly improved by the strong chemical bonding between the absorbing organic dye and metal oxide semiconductor.

DSSC [2, 3] is a sandwiched system mainly composed of a mesoporous nanocrystalline network of a wide band-gap semiconductor which is typically TiO_2, a monolayer of dye molecules (i.e. Ruthenium dye) attached on the semiconductor, a redox electrolyte which is typically I^-/I_3^- and a platinum counter electrode. Several other semiconductors such as ZnO [4, 5, 6], Nb_2O_5 [4, 5, 7-11], SnO_2 [4, 12, 13], WO_3, [5] Ta_2O_5 [5] and In_2O_3 [5] have also been used in DSSC. Figure 1.1 shows the basic structure and operating principle of DSSC. Basically, upon illumination, electrons in RuN3 dye are photo-excited to the excited states, followed by an electron injection into TiO_2 and electron diffusion through the mesoporous films and collection at TCO conducting glass. On the other hand, the photo-excited dye molecule will be regenerated by I^-/I_3^- redox system, which itself is regenerated at the counter electrode by the electron from the anode passing through the outer load.

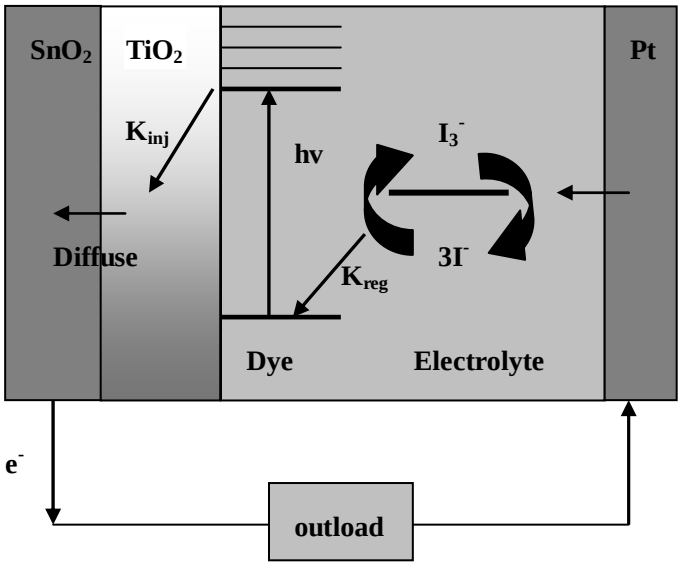

Figure 1.1 Schematic principle operation of dye-sensitized solar cell

As key processes within the operation of DSSC, charge separation and transfer along the interface between light harvesting materials and charge transport materials become extremely important since they would directly affect the photovoltage and photocurrent which are core parameters for a solar cell [14-20]. The designing idea and development for a solar cell could be directed and benefit greatly from study of the interfacial electron transfer (ET) dynamics between molecular adsorbates and wide band-gap semiconductor nanoparticles. However, unfortunately, this fundamental electron transfer process is still poorly understood [21, 22] compared with those electron transfer processes within homogeneous solution because of the obstacle from the interfacial nature of such processes.

Recently, with the rapid development in the preparation and characterization of nano-size semiconductor particles with quantum size confinement and large surface area characteristics [23], time-resolved laser spectroscopy techniques such as transient absorption and fluorescence lifetime measurement have been applied to the investigation of interfacial electron transfer dynamics between adsorbates and wide band-gap semiconductor systems [24-38]. However, although much insight has been gained, troubles still exist within these techniques. Transient absorption visible and near-IR spectroscopy are often hindered by the spectral overlap of absorption in diversified electronic states such as excited states, ground states and oxidized states. While on the other hand, time resolved fluorescence decay studies are often troubled by the non electron transfer pathways like energy transfer, moreover, dynamic fluorescence stokes shift is another obstacle to be cleared.

Ultrafast infrared transient spectroscopy [39], as a new in-situ technique which could unambiguously assign the electron process, provide the opportunity to systematically investigate the electron transfer process within the heterogeneous interface, because dynamics of electrons in the semiconductor as well as adsorbates could be directly studied [40-49]. Strong absorption of conduction band electrons and valence band holes in semiconductor originated from intraband transition between different valleys or subband could be detected, which therefore provides a direct evidence for the arrival of injected electron in the semiconductor, thereby provides a unambiguous spectroscopic probe for studying. Moreover, since ultrafast infrared transient spectroscopy is a general technique, it could be applied to various systems with different adsorbates and different semiconductors, thereby favoring a systematic study of the interfacial electron transfer dynamics.

Recently, our group [40-49, 50-53] and some other groups [54, 55] have achieved a great progress regarding the application of ultrafast transient spectroscopy to the electron transfer study. In this work, Dependence of ET on insulating metal oxide overlayer and interfacial ET between Quantum Dots and Semiconductor has been studied, which are reported in chapter 3, 4 and 5 respectively.

1.2 ET Dynamics on Adsorbates/Nanoparticles Composite

1.2.1 Dependence of ET on insulating Metal Oxide Overlayer

Both charge injection and recombination rates depend on the electronic coupling strength between the light harvesting sensitizer molecules, which serve as electron donor and

charge transport semiconductor which serve as electron acceptor. Generally, two methods were performed to control this coupling strength in order to control the charge injection and recombination processes: 1. the first approach is insertion of molecular bridging [56-59] which is well established for the study for slower electron-transfer reactions. 2. The second approach is insertion of insulating overlayers between electron donors and acceptors. Based on this consideration, various wide band-gap semiconductors such as ZrO_2 [60, 61], Al_2O_3 [60, 62, 63], MgO [61], Nb_2O_5 [64, 65], etc. have been applied to the dye sensitized solar cell. Some report has shown the conversion efficiency could be enhanced with the Al_2O_3 insulator placed between the nanoparticles. Study of the effect of Al_2O_3 on charge injection which is a major process of charge separation in dye sensitized solar cell would provide detailed insight of mechanism for the enhancement of conversion efficiency and therefore offer directions for design and modification for the solar devices. In this work, we reported the effect of Al_2O_3 and TiO_2 insulating overlayer on electron injection dynamics by using RhB, RuN3 and C343 as probe molecules. The results are presented in Chapter 3 and Chapter 4.

1.2.2 ET between Quantum Dots and Semiconductor

Quantum dot solar cell is a solar cell with quantum dots as light harvesting material and some charge transport materials, which are typically metal oxides, attached to the quantum dot to dissociate the excitons generated by photoexcitation of quantum dots followed by charge collection and conduction to produce electricity.

The reasons for quantum dots chosen as light harvesting material lies mainly in two aspects: 1. Tunable band edge of a quantum dot due to size quantization effect provide

promising opportunities in harvesting the energy in visible solar spectrum. 2. Utilization of excess energy of hot carriers in quantum dots after photoexcitation offers an original pathway to increase the photovoltage and photocurrent, which are two determinant parameters in a solar cell. Photocurrent in a quantum dot solar cell could be greatly enhanced due to the inverse Auger recombination or Impact ionization process of a quantum dot discovered and confirmed [66-69] by enormous reports from Nozik and Kilmov recently, which is actually a process to generate several excitons with one single photon by using the excess energy of photogenerated carriers to excite additional electron-hole pairs [70, 71]. With this process, thermalization (carrier cooling) problem, one of the four unavoidable losses in a solar cell paralleling incomplete absorption, recombination and thermodynamic loss, would be greatly ameliorated [72]. The quantum yield would exceed 1 if the process is active, which would theoretically enhance the photocurrent of a PV device greatly. On the other hand, photovoltage of a PV device could be enhanced with another form of utilization of the excess energy from hot carriers in which the carriers are extracted before they relax to the band edge via phonon emission, which require that the interfacial charge separation across the contacts to the semiconductor must be fast enough compared to the hot carrier cooling rate.

One of the important reasons for metal oxide material coming into consideration is the mesoporous film structure with high surface area of a metal oxide could provide a large folded support for the light harvesting material. Besides, some large-band-gap semiconductor metal oxides could accept electrons from electronically excited sensitizers, followed by electron percolation in the film with a fairly high diffusion coefficient (eg. 10^{-4} cm^2s^{-1} in TiO_2), therefore preparing metal oxide as a charge collector and conductor

in the solar cell. Apart from the reasons above, the stability of a metal oxide also makes it favorable for solar cell electrodes.

As key processes within the operation of a solar cell, especially for quantum dot solar cell which is an excitonic PV device, charge separation and transfer along the interface between light harvesting materials and charge transport materials become extremely important since they would directly affect the photovoltage and photocurrent which are core parameters for a solar cell. The designing idea and development for a solar cell could be directed and benefit greatly from study of the interfacial dynamics. Even though much study on photovoltaic effect of a quantum dot solar cell with InP, CdS and CdSe etc. as photosensitizers has been investigated in the past decade, not much detailed interfacial dynamics were reported [73-76]. Recently Kamat [77] reported the interfacial dynamics between CdSe and TiO_2 nanocomposite in the colloid form showing a wide range of rate constant values between $7.3 * 10^9$ and $1.95 * 10^{11}$ S^{-1}, which provided detailed insight for charge separation even the system was not actually same as the real working electrode.

1.3 Summary

In summary, interfacial electron transfer dynamics between adsorbate materials and mesoporous semiconductor nanoparticles could be investigated with ultrafast infrared and visible spectroscopy. Dependence of ET on insulating metal oxide overlayer and interfacial ET between Quantum Dots and Semiconductor has been studied in this work

with the framework organized as follows: Chapter 2 will summarize the procesures used for the sample preparations and measurements. Chapter 3 will discuss the effect of insulating overlayer of Al_2O_3 on the ET process within RhB-SnO_2 system by using both ultrafast infrared and visible spectroscopy. Chapter 4 will discuss the effect of insulating overlayer of TiO_2 on the ET process within RuN3-SnO_2 system and C343-SnO_2 by using both ultrafast transient infrared spectroscopies. Chapter 5 will discuss ET between Quantum Dots CdSe and Semiconductor TiO_2 by using both ultrafast infrared and visible spectroscopy.

References:

[1] Shah, A.; Torres, p.; Tscharner, R.; Wyrsch, N.; Keppner, H. Science **1999**, 285, 692.

[2] O'Regan, B.; Gratzel, M. Nature **1991**, 353, 737.

[3] Bach, U.; Lupo, D.; Comte, P.; Moser, J. E.; Weissortel, F.; Salbeck, J.; Spreitzer, H.; Gratzel, M. Nature **1998**, 395, 585.

[4] Hara, K.; Horiguchi, T.; Kinoshita, T.; Sayama, K.; Sugihara, H.; Arakawa, H. Sol. Energy Mater. Sol. Cells **2000**, 64, 115.

[5] Sayama, K.; Sugihara, H.; Arakawa, H. Chem. Mater **1998**, 10, 3825.

[6] Rensmo, H.; Keis, K.; Lindstrom, H.;Sodergren, S.; Solbrand, A.; Hagfeldt, A.; Lindquist, S. E.; Wang, L. N.; Muhammed, M. J. Phys. Chem. 1997, 101, 2598.

[7] Aegerter, M. A. Sol. Energy Mater. Sol Cells 2001, 68, 401.

[8] Aegerter, M. A.; Schmitt, M.; Guo, Y. Int. J. Photoenergy 2002, 4, 1.

[9] Hu, L. L.; Wolf, M.; Gratzel, M.; Jiang, Z. H. J. Sol-Gel Sci. Technol. 1995, 5, 219.

[10] Barros Filho, D. d. A.; Abreu Filho, P. P.; Werner, U.; Aegerter, M. A. J. Sol-Gel Sci. Technol. 1997, 8, 735.

[11] Lenzmann, F.; Krueger, J.; Brunside, S.; Brooks, K.; Graetzel, M.; Gal, D.; Ruehle, S.; Cahen, D. J. Phys. Chem. B 2001, 105, 6347.

[12] Bedja, I.; Hotchandani, S.; Kamat, P. V. J. Phys. Chem. 1994, 98, 4133.

[13] Ferrere, S.; Zaban, A.; Gregg, B. A. J. Phys. Chem. B 1997, 101, 4490.

[14] Hagfeldt, A.; Gratzel, M. Chem. Rev. 1995, 95, 49.

[15] Miller, R. J. D.; McLendon, G. L.; Nozik, A. J.; Schmickler,W.; Willig, F. Surface electron transfer precesses; VCH publishers, Inc., 1995.

[16] Kamat, P. V. Chem. Rev. 1993, 93, 267.

[17] Nazeeruddin, M. K**.** Coord. Chem. Rev. 2004, 248, 1161.

[18] Anderson, N. A.; Lian, T. Ann. Rev. Phys. Chem. 2005, 56, 491.

[19] Asbury, J. B.; Hao, E.; Wang, Y.; Ghosh, H. N.; Lian, T. J. Phys. Chem. B 2001, 105, 4545.

[20] Watson, D. F.; Meyer, G. J. Annu. Rev. Phys. Chem. 2005, 56, 119.

[21] Nozik, A, J.; Memming, R. J. Phys. Chem. 1996, 100, 13061.

[22] Lewis, N. S. Ann. Rev. Phys. Chem. 1991, 42, 543.

[23] Weller, H.; Eychmuller, A. Preparation and Characterization of Semiconductor Nanoparticles. In Semiconductor Nanoclusters: Physical, Chemical, and Catalytic Aspects; Kamat, P. V., Meisel, D., Eds.; Elsevier: Amsterdam, 1997; pp 5-22.

[24] Hannappel, T.; Burfeindt, B.; Storck, W.; Willig, F. J. Phys. Chem. B 1997, 101, 6799-6802.

[25] Nozik, A. J.; Ellingson, R. J.; Meieer, A.; Kocha, S.; Smith, B. B.; Hanna, M. Proceedings of the 21st DOE Solar Photochemistry Research Conference, June 7-11, 1997; National Technical Information Service: Springfield, VA, 1997; p 9.

[26] Martini, I.; Hartland, G. V.; Kamat, P. V. J. Phys. Chem. B 1997, 101, 4826-4830.

[27] Martini, I.; Hodak, J. H.; Hartland, G. V.; Kamat, P. V. J. Chem. Phys. 1997, 107, 8064.

[28] Cherepy, N. J.; Smestad, G. P.; Gratzel, M.; Zhang, J. Z. J. Phys. Chem. B 1997, 101, 9342.

[29] Tachibana, Y.; Moser, J. E.; Gratzel, M.; Klug, D. R.; Durrant, J. R. J. Phys. Chem. 1996, 100, 20056-20062.

[30] Rehm, J. M.; McLendon, G. L.; Nagasawa, Y.; Yoshihara, K.; Moser, J.; Gratzel, M. J. Phys. Chem. 1996, 100, 9577-9578.

[31] Lanzafame, J. M.; Miller, R. J. D.; Muenter, A.; Parkinson, B. J. Phys. Chem. 1992, 96, 2820.

[32] Eichberger, R.; Willig, F. Chem. Phys. 1990, 141, 159-173.

[33] Blackbourn, R. L.; Johnson, C. S.; Hupp, J. T. J. Am. Chem. Soc. 1991, 113, 1060.

[34] Burfeindt, B.; Hannapel, T.; Storck, W.; Willig, F. J. Phys. Chem. 1996, 100, 16463.

[35] Liu, D.; Fessenden, R. W.; Hug, G. L.; Kamat, P. V. J. Phys. Chem. B 1997, 101, 2583-2590.

[36] Murakoshi, K.; Yanagida, S.; Capel, M.; Castner, J. E. W. ACS Symp. Ser. 1997, 679, 221.

[37] Haque, S. A.; Tachibana, Y.; Klug, D. R.; Durrant, J. R. J. Phys. Chem. B 1998, 102.

[38] Yan, S. G.; Hupp, J. T. J. Phys. Chem. B 1997, 101, 1493-1495.

[39] Owrutsky, J. C.; Raftery, D.; Hochstrasser, R. M. Annu. ReV. Phys. Chem. 1994, 45, 519-555.

[40] Ghosh, H. N.; Asbury, J. B.; Weng, Y.; Lian, T. J. Phys. Chem. B 1998, 102, 10208-10215.

[41] Ghosh, H. N.; Asbury, J. B.; Lian, T. J. Phys. Chem. B 1998, 102, 6482-6486.

[42] Weng, Y.-X.; Wang, Y.-Q.; Asbury, J. B.; Ghosh, H. N.; Lian, T. J. Phys. Chem. B 2000, 104, 93-104.

[43] Ellingson, R. J.; Asbury, J. B.; Ferrere, S.; Ghosh, H. N.; Sprague, J. R.; Lian, T.; Nozik, A. J. J. Phys. Chem. B 1998, 102, 6455-6458.

[44] Asbury, J. B.; Ghosh, H. N.; Ellingson, R. J.; Ferrere, S.; Nozik, A. J.; Lian, T. Ultrafast Phenomena XI; Springer Series in Chemical Physics; Springer: Berlin, Germany, 1998; p 639.

[45] Asbury, J. B.; Wang, Y.; Lian, T. J. Phys. Chem. B 1999, 103, 6643-6647.

[46] Ellingson, R. J.; Asbury, J. B.; Ferrere, S.; Ghosh, H. N.; Sprague, J. R.; Lian, T.; Nozik, A. J. Z. Phys. Chem. (Muenchen) 1999, 212, 77-84.

[47] Asbury, J. B.; Ellingson, R. J.; Ghosh, H. N.; Ferrere, S.; Nozik, A. J.; Lian, T. J. Phys. Chem. B 1999, 103, 3110-3119.

[48] Asbury, J. B.; Hao, E.; Wang, Y.; Lian, T. J. Phys. Chem. B 2000, 104, 11957-11964.

[49] Wang, Y.; Asbury, J. B.; Lian, T. J. Phys. Chem. A 2000, 104, 4291-4299.

[50] Ai, X.; Anderson, N. A.; Guo, J.; Lian, T. J. Phys. Chem. B 2005, 109, 7088.

[51] Guo, J.; She, C.; Lian, T. J. Phys. Chem. B 2005, 109, 7095.

[52] Guo, J.; Stockwell, D.; Ai, X.; Anderson, N. A.; Lian, T. J. Phys. Chem. B 2006, 110, 5238.

[53] She, C.; Anderson, N. A.; Guo, J.; Liu, F.; Goh, W.-H; Chen, D.-T; Mohler, D. L.; Tian, Z.-Q.; Hupp, J. T.; Lian, T. J. Phys. Chem. B 2005, 109, 19345.

[54] Heimer, T. A.; Heilweil, E. J. Ultrafast Phenomena XI, 1998.

[55] Heimer, T. A.; Heilweil, E. J. Bull. Chem. Soc. Jpn. 2002, 75, 899.

[56] Smalley, J. F.; Finklea, H. O.; Chidsey, C. E. D.; Linford, M. R.; Creager, S. E.; Ferraris, J. P.; Chalfant, K.; Zawodzinsk, T.; Feldberg, S. W.; Newton, M. D. J. Am.Chem. Soc.2003, 125, 2004.

[57] Gu, Y.; Waldeck, D. H. J. Phys. Chem. B 1998, 102, 9015.

[58] Jordan, K. D.; Paddon-Row, M. N. Chem. ReV. 1992, 92, 395.

[59] Nitzan, A.; Ratner, M. A. Science 2003, 300, 1384.

[60] Palomares, E.; Clifford, J. N.; Haque, S. A.; Lutz, T.; Durrant, J. R. J. Am. Chem. Soc. 2003, 125, 475.

[61] Kay, A.; Graetzel, M. Chem. Mater. 2002, 14, 2930.

[62] Alarcon, H.; Boschloo, G.; Mendoza, P.; Solis, J. L.; Hagfeldt, A. J. Phys. Chem. B 2005, 109, 18483.

[63] O'Regan, B. C.; Scully, S.; Mayer, A. C.; Palomares, E.; Durrant, J. J. Phys. Chem. B 2005, 109, 4616.

[64] Zaban, A.; Chen, S. G.; Chappel, S.; Gregg, B. A. Chem. Commun. (Cambridge, U.K.) 2000, 2231.

[65] Chen, S. G.; Chappel, S.; Diamant, Y.; Zaban, A. Chem. Mater. 2001, 13, 4629.

[66] Schaller, R. D.; Klimov, V. I. *Phys. Re*v. *Lett.* **2004**, *92*, 186601-186604.

[67] Schaller, R. D.; Sykora, M.; Pietryga, J. M.; Klimov, V. I. *Nano Lett.* **2006**, 6, 424-429.

[68] Shabaev, A.; Efros, A. L.; Nozik, A. J. *Nano Lett.* **2006**, 6, 2856-2863.

[69] Nozik, A. J. *Physica E* **2002**, *14*, 115-120.

[70] P.T. Landsberg, H. Nussbaumer, G. Willeke, J. Appl. Phys. 1993, 74, 1451.

[71] S. Kolodinski, J.H. Werner, T. Wittchen, H.J. Queisser, Appl. Phys. Lett. 1993, 63, 2405.

[72] M. C. Hanna and A. J. Nozika 2006 J Appl Phys, 100, 074510

[73] Zaban, A.; Micic, O. I.; Gregg, B. A.; Nozik, A. J, Langmuir; (Letter), 1998; 14(12); 3153-3156

[74] Vogel, R.; Weller, H. *J. Phys. Chem*. **1994**, *98*, 3183.

[75] Weller, H. *Ber. Bunsen-Ges. Phys. Chem.* **1991**, *95*, 1361.

[76] Hoyer, P.; Konenkamp, R. *Appl. Phys. Lett*. **1995**, *66*, 349.

[77] István Robel, Vaidyanathan Subramanian, Masaru Kuno, and Prashant V. Kamat J. 2006, Am. Chem. Soc., 128 (7), 2385 -2393.

Chapter 2 Experimental Section

The samples prepared in this work are based on metal oxide nanoporous films and quantum dot CdSe nanoparticles. Synthesis of semiconductor colloid and films and quantum dot CdSe nanoparticles are based on published procedures with slight modification. Electron injection dynamics were investigated with ultrafast pump and probe transient infrared and visible absorption spectroscopy as well as the time resolved fluorescence spectroscopy. Photostability of the nanocomposite was investigated with UV-vis spectrophotometer. This chapter provides a summarization of the procesures used for the sample preparations and measurements.

2.1 Preparation of Semiconductor Colloid, Nanoporous Films and Nanocomposites

2.1.1 Preparation of TiO_2 Colloid and Films

TiO_2 nanocrystalline thin films were prepared by a sol-gel method followed by growth under hydrothermal condition, similar to that used by Zaban.[1] Briefly, 250 mL of water and 80 mL of acetic acid were mixed into a 1000 mL round bottom flask under ice bath. A mixture of 10 mL of 2-propanol and 37 mL of titanium (IV) isopropoxide (Aldrich, 97%) was then dropped slowly to the acetic acid solution over a 30-40 min period under vigorous stirring and dry N_2 purge. After stirring overnight, the transparent

colloid was poured into a 1000 ml beaker and heated in 80°C hot water bath for 3-4 h under vigorous stirring.

The resulting gel was autoclaved at 230°C for 12 h and cooled down to room temperature slowly. Autoclaving allows controlled colloid hydrothermal growth through Ostwald ripening, whereby smaller particles dissolve and fuse to larger ones.[2] Burnside et al.[3] have shown that both particle size and porosity of films increased with increasing autoclaving temperature, however, the surface area decreased. They also found that the films autoclaved below 230°C had the ordered structures and narrow pore size distributions. Therefore, 230°C was used as autoclaving temperature in all our TiO_2 colloid preparation. During the autoclaving, the gel was separated into liquid and solid phases. The solid phase was then collected and stirred for several days to disperse the aggregated particles. About 20 drops of TritonX-100 (Aldrich) was added to ~10 mL colloid to facilitate the spreading before stirring.

2.1.2 Preparation of SnO_2 Colloid and Films

Colloidal SnO_2 was synthesized according to a published procedure.[4] 85 mmol (~10 ml) of $SnCl_4$ (99.9%, Aldrich) was injected into 20 mL of HCl (37 wt. %) by syringe and was then dispersed in the HCl by using ultrasonic for at least 30 minutes. The resulting solution was added drop-wise into 500 mL of water under rapid stirring at 0°C. After stirring for 30 min, aqueous ammonia (25%) was added to the solution until a pH value of 3.5 - 4.0 was reached, which led to precipitate of SnO_2 nanoparticles. The solution was allowed to settle overnight in the dark and white precipitate was observed during the sintering process. The precipitate was then washed at least 3 times with distilled water,

and then 300 mL of water was added and the pH value was adjusted to 9.5-10, stirred vigorously overnight, and dialyzed against ~10 L of water at pH 10 for at least two days. The resulting transparent SnO_2 colloid was then refluxed for 4 h. A 150 ml of this colloid was poured into an autoclave and heated firstly at 150°C for 1 h, then at 270°C for 16 h. The solution was concentrated to 50 mL by rotorvaporing under vacuum. Then 5 ml of the solution and 2 drops of TritonX-100 were mixed and stirred for at least 1 day. The solution was then cast onto sapphire substrates, dried in air, and baked at 400°C for 1h. The samples were then allowed to slowly return to room temperature.

2.1.3 Preparation of ZrO_2 Films

ZrO_2 nanoparticles were obtained from Degussa Corporation, and the thin films were prepared according to the published procedure [5]. ZrO_2 powder (2g) was ground in a mortar with distilled water (4 ml), acetylacetone (10 ul) and 5 drops of Triton X-100 to break up the aggregate into a dispersed paste. Adhesive tape was placed on the edges of the polished sapphire windows to form a guide for spreading the slurry using a glass rod. After being dried in air, the film was baked at 400 ^{o}C for 60 min in air.

2.1.4 Preparation of RhB-Al_2O_3- SnO_2 Nanocomposite

Preparation of Al_2O_3 Overlayer on SnO_2 films

The colloid SnO_2 particles and nanocrystalline thin films were prepared following the above. The Al_2O_3 coating layers were prepared according to published literatures [6, 7]. Briefly, the newly prepared SnO_2 films were first dried at 120^{o}C to remove excess free water, followed by immersion of the films into 0.15 M Al(Bu^{i}O)3 solution with the

solvent isopropanol for 15 min at 55°C. After immersion, the films were immediately washed by isopropanol three times, hydrolyzed in water and baked at 400 °C for 60 min. The number of Al_2O_3 overlayers was controlled according to the number of repeating immersing/sintering cycles. All nanocrystalline films were sintered for the same amount of time in total to minimize the sintering effect.

Sensitization of SnO_2 thin films

The SnO_2 films covered with different overlayers of Al_2O_3 were directly immersed into RhB dye solution for 30---60 min the absorption.

2.1.5 Preparation of RuN3-TiO_2- SnO_2 and C343-TiO_2- SnO_2 Nanocomposites

Preparation of TiO_2 Overlayer on SnO_2 films

The colloid SnO_2 particles and nanocrystalline thin films were prepared following the above. The coating layers were prepared according to published literatures [8]. Briefly, the newly prepared SnO_2 films were first dried at 120°C to remove excess free water, followed by immersion of the films into 0.09 M $TiCl_4$ solution with the solvent water for 24 hours at room temperature. The resulting film was washed by distilled water thoroughly and sintered for 1 hour at 400 °C. The number of **TiO_2** overlayers was controlled according to the number of repeating immersing/sintering cycles.

Sensitization of SnO_2 thin films

The SnO_2 films covered with different overlayers of **TiO_2** were directly immersed into C343 dye solution for 30---60 seconds and N3 dye solution for about 2 minutes for the absorption

2.1.6 Preparation of TiO_2-CdSe and ZrO_2-CdSe nanocomposite

Synthesis of thiol-capped CdSe.

Thiol-capped CdSe were synthesized by established literature procedure with little modifications [9]. Briefly, 90ul MPA and 20ml methanol were mixed with the pH adjusted to 10.9 with tetramethylammonium hydroxide. Under dark condition, 40mg TOPO capped CdSe were dissolved in the mixure under nitrogen flow. The vessel was refluxed overnight at 65^{o}C. The final solution was washed by ethyl acetate two times to delete TOPO.

Synthesis of dithiocarbamate-capped CdSe.

Dithiolcarbamate-capped CdSe were synthesized with the procedure from the established literature [10]. Briefly, 100 nmol CdSe were precipitated in MeOH with the supernatant discarded. The precipitated CdSe were then redissolved in a 3ml MeOH/$CHCl_3$ mixure (1:1). In another flask, 1.06 mmol glycine, 384 mg tetramethyammonium hydroxide pentahydrate and 1.06 mmol CS_2 were mixed together to react in 2 ml MeOH/$CHCl_3$ mixure (1:1). The solution of CdSe was then added to the latter and stirred for 12 hours at room temperature. Afterwards, 5 ml diethylether was added to precipitate the QDs which were isolated by centrifugation. The supernatant was discarded and the CdSe was rewashed by methonal and THF. The resulting solid was dissolved in methonal.

Preparation of TiO_2-CdSe and ZrO_2-CdSe nanocomposite

TiO_2 and ZrO_2 nanoporous thin films were prepared based on the published procedures. The films then were dipped in the thiol-capped CdSe, dithiocarbamate-capped CdSe and TOPO-capped CdSe solution for several hours for the film sensitization.

TiO_2 nanoporous thin film, first stored in an oven (373K), was immediately moved to a 20mM MPA solution in acetonitrile for 4 hours. The resulting film was washed by acetonitrile and heptane subsequently and then immersed in CdSe solution in heptane for 12 hours.

2.2. Sensitizers Used in This Work

2.2.1 Rhodamine B and Coumarin 343

Rhodamine B and Coumarin 343 were purchased from Aldrich. Both dyes contain carboxylic groups which are believed to be a bounding group to the semiconductor. Figure 2.1 shows the schematic structure of Rhodamine B and Coumarin 343.

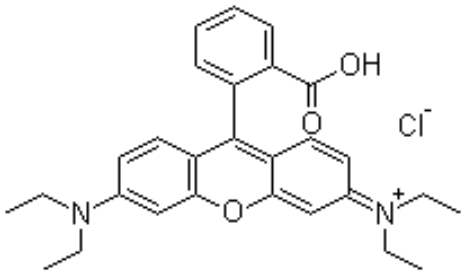

(a)

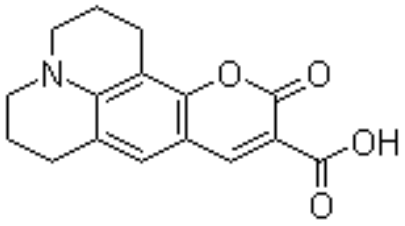

(b)

Figure 2.1 Molecular structure of RhB and C343. (a) Molecule structure of RhB. (b) Molecule structure of C343

2.2.2 RuN3 dye

High purity compounds $Ru(dcbpyH2)_2(SCN)_2$ (dcbpy = 2,2'-bipyridine-4,4'-dicarboxylate) is called RuN3, which for our experiment is purchased from Solaronix (Lausanne, Switzerland). Figure 2.2 shows the schematic structure of RuN3. The carboxyl ate groups prepare RuN3 easily attaching to metal oxide semiconductor through the relatively tight chemical bonding.

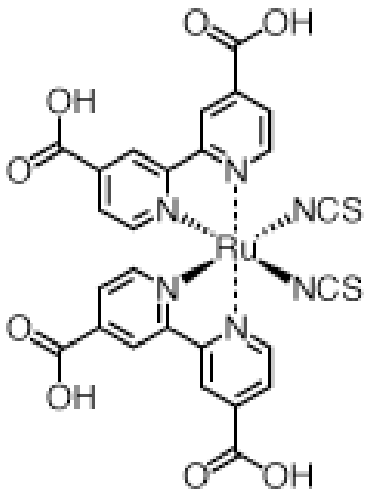

Figure 2.2 Molecular structure of RuN3

2.3 Photostability study with a UV-vis spectrophotometer

Different CdSe solutions and TiO_2-CdSe nanocomposite were put in UV-vis spectrophotometer. The UV-vis spectra were recorded at certain time intervals. The temporal evolutions of the optical density at the exciton absorption peak were calculated from the spectra.

2.4 Ultrafast Transient Absorption Measurement

2.4.1 Ultrafast Infrared Transient Absorption Measurement

The Ultrafast Infrared Transient Absorption measurement in our experiment were performed in a pump-probe scheme, which has been described in detail previously [11-15] .Briefly, the infrared spectrometer in our experiment is controlled by the Coherent Legend laser system (800 nm, 150 fs, 2.5 mJ/pulse) and two optical parametric amplifiers (OPA).

As for the probe pulses, an IR OPA is first pumped by 800 nm pulses to produce the signal and idler output, which then were difference-frequency mixed in an AgGaS2 crystal, where the tunable mid-IR probe pulses with a full width at half-maximum (FWHM) of ～120 cm-1 is produced. For the pump pulses, an IR OPA is pumped by 800 nm of 1mJ pulses to produce the signal and idler output, which then were collinearly mixed with a fundamental in BBO crystal, where the tunable pump pulses are produced.

In our experiment, SnO_2- Al_2O_3-RhB nanocomposite was pumped at 532nm, while SnO_2-TiO_2-N3 and SnO_2- TiO_2-C343 were pumped at 400nm. The pump power for SnO_2-TiO_2-N3, SnO_2- TiO_2-C343 and SnO_2- Al_2O_3-RhB were 683nJ, 338nJ and 75nJ respectively. In the light path, a wheel ND filter can be arranged to tune the energy of the pump pulses. At the sample, the beam diameters of pump and probe pulses are ～250 and 180 um respectively. To facilitate the detection with a 32-element mercury cadmium telluride (MCT) array detector, the probe beam after the sample was dispersed in a spectrometer. During the data collection, samples were constantly translated at a speed around 5 mm/min to avoid permanent photo-damage.

2.4.2 Ultrafast Visible Transient Absorption Measurement

The visible pump-probe set up used for our studies was based on a regeneratively amplified femtosecond Ti:sapphire laser system (1 kHz repetition rate at 800 nm, 100 fs, 950 μJ/pulse). The 800 nm output pulse from the regenerative amplifier was split into two parts to generate pump and probe pulses. One part, with 350 uJ/pulse, was used to generate pump pulses at 400 nm by Second Harmonic Generation (SHG), and focused on the sample with a beam diameter of 400 nm and energy 130nJ/pulse. The visible probe was generated by attenuating and focusing ~10 μJ of the fundamental into a 2 mm sapphire window to produce a white light continuum with a range of 420 nm to 750 nm. The probe was focused on the sample to a spot size of 100 μm. After the sample, the probe was focused into a fiber-coupled spectrometer (Ocean Optics USB2000, 2048 pixel CCD, ~.25 nm/pixel readout) and detected at a frequency of 100 Hz. The pump pulses were synchronously blocked by a chopper at the same frequency, and the absorbance change was calculated by comparing the probe intensity with pump on and blocked. The

pump power in our experiment was 25 nJ for the SnO_2- Al_2O_3-RhB. The zero time delay and instrument response function of the measurement were obtained with the instantaneous ground state bleach at 550 nm of Ruthenium polypyridyl complex in ethanol solution.

2.5 Fluorescence lifetime measurements.

Time–resolved fluorescence measurements were performed in the time-correlated single photon counting (TCSPC) mode under right-angle sample geometry. A femtosecond laser pulse (100 fs) with a repetition rate of 80 MHz was generated from a mode-locked Ti:Sapphire laser (Tsunami oscillator pumped by 10 W Millennia Pro, Spectra-Physics). The output centered at 800 nm was doubled through a BBO crystal to generate 400 nm light that was used to excite the sample. The emission was detected by a Micro-channel-plate-photomultiplier tube (Hamamatsu R3809U-51), whose output was amplified and analyzed by a TCSPC board (Becker&Hickel SPC 600).

Reference

[1] Zaban, A.; Ferrere, S.; Sprague, J.; Gregg, B. A. J. Phys. Chem. B 1997, 101, 55.

[2] Kalyanasundaram, K.; Gratzel, M. Coord. Chem. Rev. 1998, 177,347.

[3] Nutz, T.; Felde, U. Z.; Haase, M. J. Chem. Phys. 1999, 110, 12142.

[4] Lenzmann, F.; Shklover, V.; Brooks, K.; Gratzel, M. J. Sol-Gel Sci. Technol. 2000, 19, 175.

[5] Nozik, A. J.; Memming, R. J. Phys. Chem. 1996, 100, 13601.

[6] Palomares, E.; Clifford, J. N.; Haque, S. A.; Lutz, T.; Durrant, J. R. J. Am. Chem. Soc. 2003, 125, 475.

[7] Palomares, E.; Clifford, J. N.; Haque, S. A.; Lutz, T.; Durrant, J. R. Chem. Commun. (Cambridge, U.K.) 2002, 1464.

[8] Kim, K; Benkstein, K. D; van de Lagemaat, J; Frank, A. J. Chem. Mater. 2002, 14, 1042-1047.

[9] Aldana, J.; Wang, Y. A.; Peng, X, J. Am. Chem. Soc.; (Article); 2001; 123(36); 8844-8850.

[10] Fabien Dubois, Benoıˆt Mahler, Benoıˆt Dubertret, Eric Doris, and Charles Mioskowski, J. AM. CHEM. SOC. 2007, 129, 482-483

[11] Asbury, J. B.; Anderson, N. A.; Hao, E.; Lian, T. J. Phys. Chem. B 2003, 107, 7376.

[12] Guo, J.; Stockwell, D.; Ai, X.; She, C.; Anderson, N. A.; Lian, T. *J. Phys. Chem. B* 2006, 110, 5238.

[13] Ai, X.; Anderson, N. A.; Guo, J.; Lian, T. J. Phys. Chem. B 2005, 109, 7088.

[14] Ai, X.; Guo, J.; Anderson, N. A.; Lian, T. J. Phys. Chem. B 2004, 108, 12795.

[15] Guo, J.; She, C.; Lian, T. J. Phys. Chem. B. 2005, 109, 7095.

Chapter 3 Dependence of Electron transfer on Insulating Al_2O_3 Overlayer in RhB-SnO_2 films

Electron injection process, as a main charge separation process which plays an extremely important role on the conversion efficiency of a dye sensitized solar cell, could be controlled with insertion of insulating overlayers between electron donors and acceptors along the nanoparticle interface. In this work, SnO_2 with the dye Rhodamine-B (RhB) attached was chosen as a dye sensitized semiconductor system for the study of effect of insulating overlayer of Al_2O_3 on the electron injection process because injection dynamics of RhB-SnO_2 system was expected to be relatively fast enough to be completed within 1ns detection time window, which would greatly facilitate our comparison among injection dynamics. Moreover, ultrafast transient visible experiment could be applied in this system since cation position as well as excited state position of RhB was clearly assigned during our past study. We have shown that electron injection dynamics was slowed down for the RhB-SnO_2 film with the increase of the number of Al_2O_3 overlayer from the transient IR signal which is attributed to electrons in the conduction band of SnO_2, while from the transient visible experiment, a corresponding slowing down of the cation formation of RhB was observed.

Dye sensitized solar cell [1], which achieves optical absorption and the subsequent charge separation by linking a wide band gap semiconductor with a light harvesting material, has receive extensive attention with its cost-effective characteristics. As key processes within the operation of a dye sensitized solar cell, charge separation along the interface between

light harvesting materials and charge transfer semiconductors become extremely important since they would directly affect the photovoltage and photocurrent which are core parameters for a solar cell, which makes charge injection and recombination which are two main components of charge separation process become focus for the interfacial dynamic investigation.

Both charge injection and recombination rates depend on the electronic coupling strength between the light harvesting sensitizer molecules, which serve as electron donor and charge transport semiconductor which serve as electron acceptor. Generally, two methods were performed to control this coupling strength in order to control the charge injection and recombination processes: 1. The first approach is insertion of molecular bridging [2-5] which is well established for the study for slower electron-transfer reactions. 2. The second approach is insertion of insulating overlayers between electron donors and acceptors. Based on this consideration, various wide band-gap semiconductors such as ZrO_2 [6, 7], Al_2O_3 [6, 8, 9], MgO [7], Nb_2O_5 [10, 11], etc. have been applied to the dye sensitized solar cell. Some report has shown the conversion efficiency could be enhanced with the Al_2O_3 insulator placed between the nanoparticles. Study of the effect of Al_2O_3 on charge injection which is a major process of charge separation in dye sensitized solar cell would provide detailed insight of mechanism for the enhancement of conversion efficiency and therefore offer directions for design and modification for the solar devices.

In our experiment, the effect of insulating overlayers on electron injection dynamics by using RhB as probing dyes. In our RhB- Al_2O_3-SnO_2 system, RhB was chosen because injection dynamics of RhB-SnO_2 system was expected to be relatively faster and would be completed within 1ns, which could greatly facilitate our comparison among injection

dynamics. Moreover, we could also investigate the cation formation kinetics of RhB in this system with ultrafast transient visible experiment since cation position as well as excited state position of RhB was clearly assigned during our past experiment, therefore provide us a double confirmation opportunity for the injection dynamics. We have observed apparent difference of electron injection dynamics from RhB to SnO_2 between films with and without insulating overlayer. With the increasing of the number of Al_2O_3 overlayer, a slowing down of the electron injection was observed.

Results

3.1 Ultrafast Infrared Transient Absorption measurement for RhB- Al_2O_3-SnO_2

Electron injection dynamics from RhB to SnO_2 with 0, 1, 2 and 3 insulating Al_2O_3 overlayer were monitored with transient mid-IR absorption measurement. RhB was first excited by 532nm pump beam, followed by electron injection into conduction band of SnO_2, where the injected electrons were probed with ranging from 1905 to 2072 wave numbers. Figure 3.1 shows the UV-vis absorption spectra of RhB- SnO_2 films with 0-3 insulating Al_2O_3 layers. Figure 3.2 shows the electron injection dynamics scaled to the same number of absorbed photons at 532nm which is the pump position.

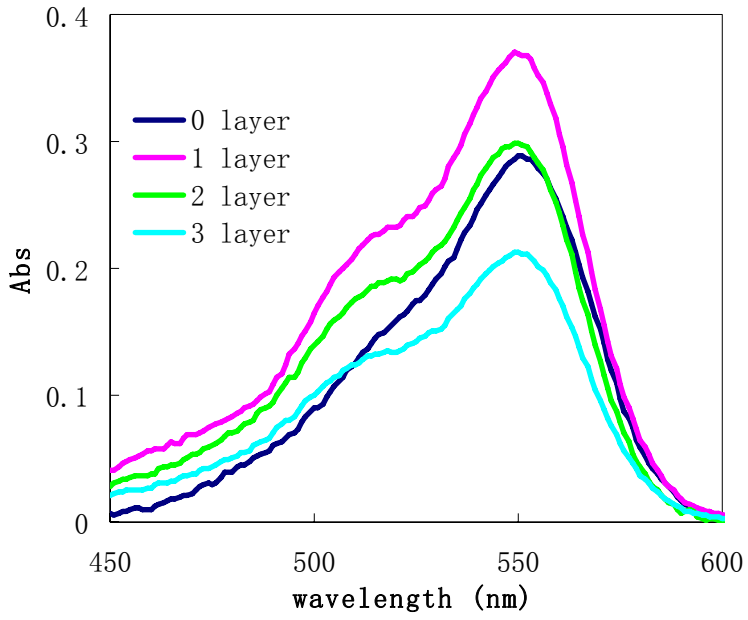

Figure 3.1 UV-vis absorption spectra of RhB- SnO_2 films with 0-3 insulating Al_2O_3 layers.

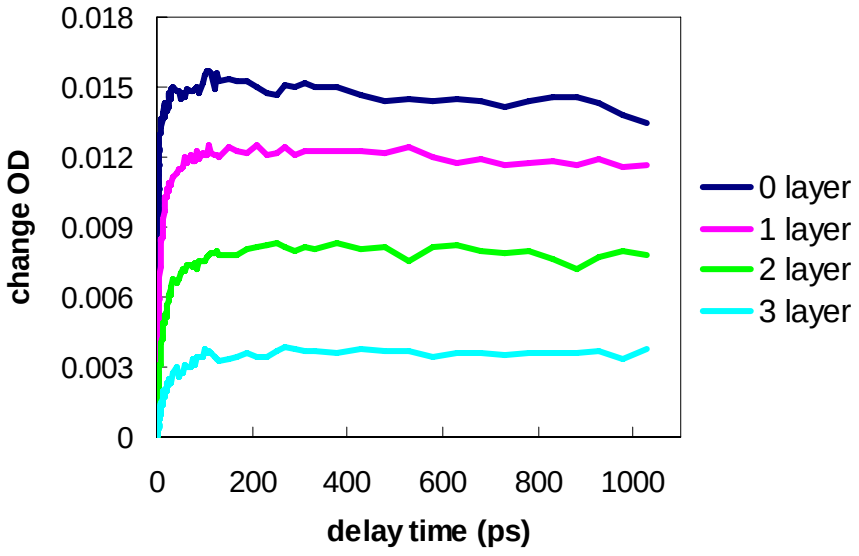

Figure 3.2 Comparison of the transient IR absorption dynamics for the RhB- SnO_2 films with 0-3 insulating Al_2O_3 layers after correction of the absorption at 532nm to the same number of absorbed photons.

We could achieve from figure 3.2 the entire electron injection dynamics were complete within 1ns. With the increasing of numbers of insulating Al_2O_3 layers, the injection yield become smaller and smaller.

Since all the kinetics are complete within the 1ns detection time window, we could compare the injection kinetics easily by normalizing them to the very end of delay time, which makes the RhB dye, unlike ReClA and RuN3 dyes whose injection dynamics could not be finished within 1ns in the dye- Al_2O_3 -SnO_2 system, more appropriate to be applied for the comparison of injection kinetics. Figure 3.3 Comparison of the transient IR absorption signal for the RhB- SnO_2 films 0, 1, 2 and 3 insulating Al_2O_3 layers probed at 1905-2072 cm^{-1}

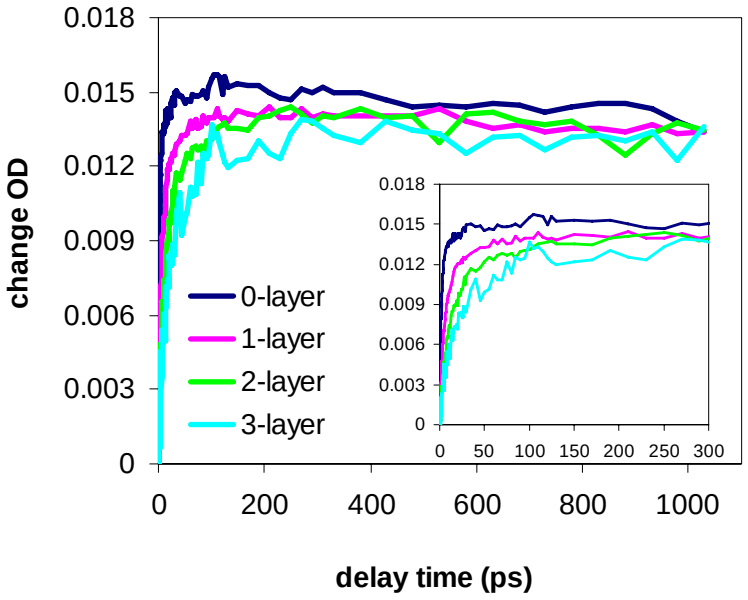

Figure 3.3 Comparison of the transient IR absorption signal for the RhB- SnO_2 films with 0-3 insulating Al_2O_3 layers normalized at the delay time of 1029 ps. The inset panel shows the same dynamics in the 300ps time window.

It is apparent from the data that with the increasing number of insulating Al_2O_3 layers, the electron injection dynamics become slower. We could see that it spend roughly 40 ps for the 0-layer system to reach the maximum of the signal size, while it takes about 100ps, 250ps and 300ps for the 1L, 2L and 3L system to reach the maximum of the signal size respectively.

3.2 Ultrafast visible Transient Absorption measurement for RhB-Al_2O_3-SnO_2

Electron injection dynamics were also monitored with transient visible absorption measurement to investigate the kinetics of RhB. RhB-SnO_2 system with 0, 1 and 2 insulating Al_2O_3 overlayer was first excited by 532nm pump beam, followed by electron injection into conduction band of SnO_2, the kinetics within the visible range were recorded with ultrafast visible absorption spectroscopy. Figure 3.5 shows Ultrafast transient visible absorption spectra of RhB- SnO2 films with 0, 1 and 2 insulating Al_2O_3 layers. If we look at RhB side, we know RhB will be excited with the incident light to the excited state followed by the cation formation, which is shown in the following equation:

$$RhB \rightarrow RhB^* \rightarrow RhB^+ + e^-$$

Since cation formation and electron injection happen at the same time, we would expect the cation formation for RhB dye in this system would possess the similar tendency of dynamics to that electron signal in semiconductor observed in the transient IR absorption

spectroscopy. The excited state absorption position for RhB is around at 460nm, stimulated emission is at 570---620nm, and the cation absorption position is around 490nm.

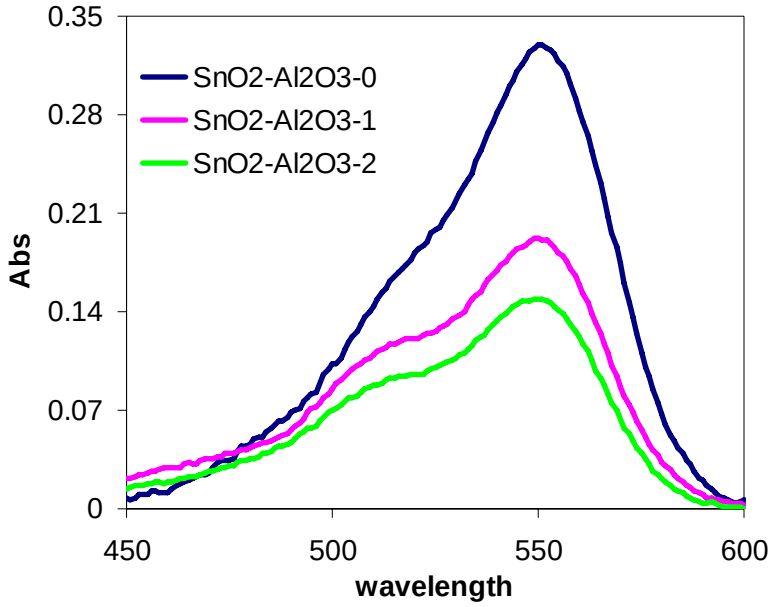

Figure 3.4 UV-vis absorption spectra of RhB-SnO_2 with 0-2 Al_2O_3 overlayers

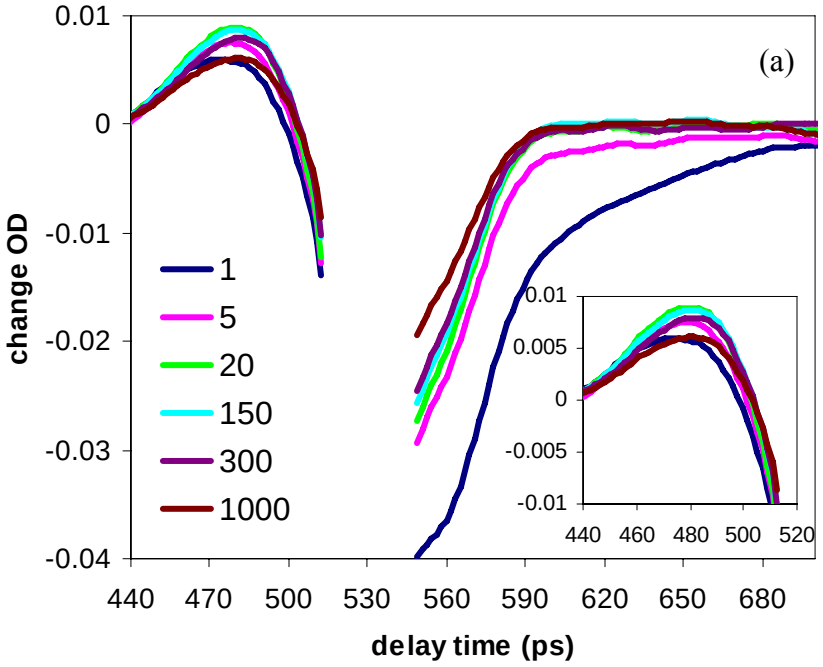

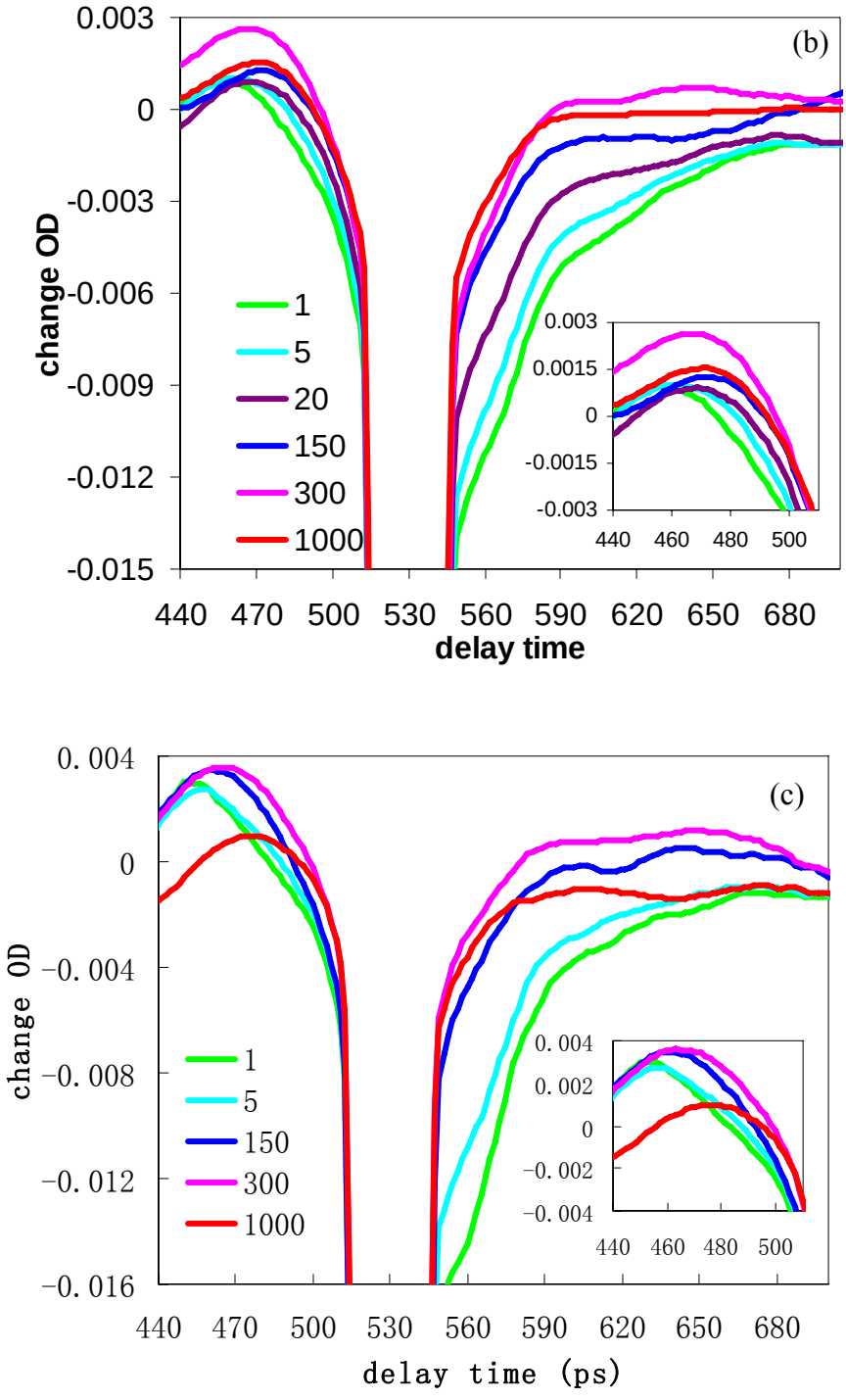

Figure 3.5 Ultrafast transient visible absorption spectra of RhB- SnO_2 films with 0-2 insulating Al_2O_3 layers**.** (a) Transient visible spectra for RhB- SnO_2 film with 0

layers. (b) Transient visible spectra for RhB- SnO_2 film with 1 insulating Al_2O_3 layer. (c) Transient visible spectra for RhB- SnO_2 film with 2 insulating Al_2O_3 layer. The insets of the three panels show the corresponding spectras around the position of RhB cation formation

From the spectra evolution shown in figure 3.5, we could observe the decay of RhB excited state (absorption at about 460nm and stimulate emission at 570—650 nm) as well as the growth of cation absorption at about 490nm. For the 0 insulating Al_2O_3 layer transient spectra, stimulated emission of RhB excited state almost decreases to zero around 5 ps and cation absorption already happens within 5ps shown in light blue curve in spectra (a). This indicates a fast electron injection from RhB to SnO_2; For 1 layer system, we could tell from spectra (b) that RhB cation absorption happens around 20 ps which is slower than 0 layer system and also the stimulated emission still exists at 20 ps; For the 2 layer system, we could tell from spectra (c) that RhB cation absorption happens around 150ps, which indicates a relatively long-lived excited state of RhB and much slower electron injection from RhB to semiconductor.

The electron injection dynamics we obtained have apparently showed that the injection rates become slower with the increasing number of insulating Al_2O_3 layers. This dependence could be attributed to the changes of electronic coupling because of the thickness increasing of insulating Al_2O_3 layers. Electron transfer rate depends on the density of states in the semiconductor because total electron transfer rate in the non-adiabatic limit is determined by the sum of the transfer rates of all the possible terminal

states. Therefore electron transfer rate could be calculated by the total rate to all the possible accepting state in the metal oxides [12-16].

$$k_{et} = \frac{2\pi}{\hbar}\int_{-\infty}^{\infty} dE[1 - f(E_f, E)]\rho\left|\overline{H(E)}\right|^2 \frac{1}{\sqrt{4\pi\lambda k_B T}} \exp[-\frac{(\lambda + \Delta G_0 + E)^2}{4\lambda k_B T}]$$

Where Δ G0 is the difference of free energy between the adsorbate excited state (electrochemical potential E (S^+/S^*)) and the conduction band edge of the metal oxide (electrochemical potential E 0 (CB)); H(ε) is the averaged electron coupling between the adsorbate excited state and all different k states in metal oxides with the same energy ε , which is defined relative to the band edge energy and thus equals to ($E-E_{CB}$); λ is the total reorganization energy; ρ (ε) is the density of states at energy ε within metal oxides; f (E_f, E) is the fermi occupancy factor which insure that electron injects into unfilled states only.

From the equation above, we could tell the electron transfer rate K_{ET} is proportional to the square of the averaged electronic coupling H(ε), which is determined by the distance between adsorbate and metal oxide in our case and also the binding strength. Generally two mechanisms are proposed for the electron transfer within a donor-bridge-acceptor system: multi-step hopping mechanism and single-step electron transfer. For the multi-step hopping mechanism, the energy level of bridge states are relatively lower or around that of the donor material, which directs the electron to go through the bridge material by multi-step hopping at states [17, 18]. On the other hand, single-step electron transfer is applied when the energy level of bridge states are much higher than that of donor and acceptor material, which prepares the electron go through the bridge material by one or more delocalized virtual states. This process is usually presenting a fast

exponential decay for the electron transfer rate and is called superexchange. In our investigated RhB- Al_2O_3 -SnO_2 system, if we assume there are no defect and trap states within the insulating Al_2O_3 overlayer the tunneling barrier for the electron transfer would be 4.5 V which is calculated from the conduction band edge of SnO_2 and Al_2O_3 : 0V and 4.5V (vs SCE) [19]. However, the real tunneling barrier in the experiment would be lower than 4.5V because there would be some defect and trap states within the insulating Al_2O_3 layer. Meanwhile, the interaction between insulating overlayer and semiconductor film should also be considered, although there is no consensus how the conduction band edge is affected by such interaction.

3.3 Summary

The dependence of electron injection dynamics on the number of Al_2O_3 insulating overlayers has been studied with ultrafast transient infrared and visible spectroscopy. The system RhB-SnO_2 was chosen because injection dynamics of RhB-SnO_2 system was expected to be relatively fast enough to be completed within 1ns detection time window, which would greatly facilitate our comparison among injection dynamics. RhB- SnO_2 systems with 0, 1, 2 and 3 L Al_2O_3 insulating overlayers were investigated with ultrafast transient infrared spectroscopy, and it is shown that with the increasing of the number of Al_2O_3 overlayers, electron injection dynamics was slowed down for the RhB-SnO_2 film, while from the transient visible experiment, a corresponding slowing down of the cation formation of RhB was observed with the increasing of the number of Al_2O_3 overlayers, which confirmed the dependence of electron injection dynamics on the number of Al_2O_3 insulating overlayers.

Reference

[1] O'Regan, B.; Gratzel, M. Nature 1991, 335, 737.

[2] Smalley, J. F.; Finklea, H. O.; Chidsey, C. E. D.; Linford, M. R.; Creager, S. E.; Ferraris, J. P.; Chalfant, K.; Zawodzinsk, T.; Feldberg, S. W.; Newton, M. D. J. Am.Chem. Soc.2003, 125, 2004.

[3] Gu, Y.; Waldeck, D. H. J. Phys. Chem. B 1998, 102, 9015.

[4] Jordan, K. D.; Paddon-Row, M. N. Chem. ReV. 1992, 92, 395.

[5] Nitzan, A.; Ratner, M. A. Science 2003, 300, 1384.

[6] Palomares, E.; Clifford, J. N.; Haque, S. A.; Lutz, T.; Durrant, J. R. J. Am. Chem. Soc. 2003, 125, 475.

[7] Kay, A.; Graetzel, M. Chem. Mater. 2002, 14, 2930.

[8] Alarcon, H.; Boschloo, G.; Mendoza, P.; Solis, J. L.; Hagfeldt, A. J. Phys. Chem. B 2005, 109, 18483.

[9] O'Regan, B. C.; Scully, S.; Mayer, A. C.; Palomares, E.; Durrant, J. J. Phys. Chem. B 2005, 109, 4616.

[10] Zaban, A.; Chen, S. G.; Chappel, S.; Gregg, B. A. Chem. Commun. (Cambridge, U.K.) 2000, 2231.

[11] Chen, S. G.; Chappel, S.; Diamant, Y.; Zaban, A. Chem. Mater. 2001, 13, 4629.

[12] Asbury, J. B.; Anderson, N. A.; Hao, E.; Lian, T. J. Phys. Chem. B, 2003, 107, 7376.

[13] Gao, Y. Q.; Georgievskii, Y.; Marcus, R. A. J. Chem. Phys. 2000, 112, 3358.

[14] Gao, Y. Q.; Marcus, R. A. J. Chem. Phys. 2000, 113, 6351.

[15] Gosavi, S.; Marcus, R. A. J. Phys. Chem. B 2000, 104, 2067.

[16] Asbury, J. B.; Hao, E.; Wang, Y.; Ghosh, H.N.; Lian, T. J. Phys. Chem. B 2001, 105, 4545.

[17] Palomares, E.; Clifford, J. N.; Haque, S. A.; Lutz, T.; Durrant, J. R. J. Am. Chem. Soc. 2003, 125, 475.

Chapter 4 Dependence of Electron transfer on Insulating TiO_2 Overlayer in RuN3-SnO_2 and C343-SnO_2 films

Electron injection process, as a main charge separation process which plays an extremely important role on the conversion efficiency of a dye sensitized solar cell, could be controlled with insertion of insulating overlayers between electron donors and acceptors along the nanoparticle interface. Post treatment of TiO_2 overlayer on the semiconductor film has been proved to enhance the performance of a DSSC [1-4]; however, the detail interfacial electron transfer process is still poorly understood. In this work, we are trying to nail out the dependence of TiO_2 overlayer on the electron transfer processes within the SnO_2-RuN3 and SnO_2-C343 systems by using ultrafast transient infrared absorption spectroscopy. SnO_2 overlayer on TiO_2 film was also tried with the ultrafast transient infrared absorption spectroscopy to provide a comparation.

Results

4.1 Ultrafast transient infrared spectroscopy of SnO_2- TiO_2 -RuN3

Electron injection dynamics from RuN3 to SnO_2 with 0, 1, 2 and 3 insulating TiO_2 overlayer were monitored with transient mid-IR absorption measurement. RuN3 was first excited by 400nm pump beam, followed by electron injection into conduction band of SnO_2, where the injected electrons were probed with ranging from 1905 to 2072 wave

numbers. Figure 4.1 shows UV-vis absorption spectra of TiO_2-N3 and SnO_2-N3 with 0-3 TiO_2 overlayers. Figure 4.2 shows the electron injection dynamics which are scaled at pump position 400nm to the same absorbed photons, allowing a comparison of injection yield of electron.

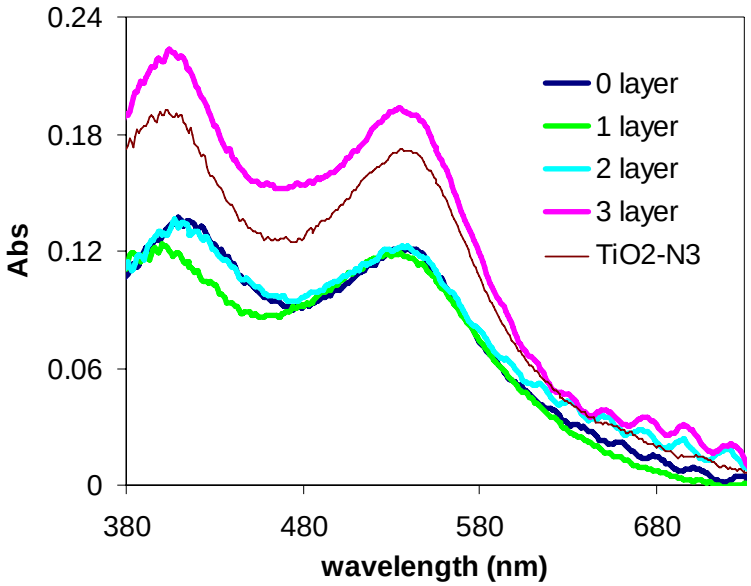

Figure 4.1 UV-vis absorption spectra of TiO_2-N3 and SnO_2-N3 with 0-3 TiO_2 overlayers

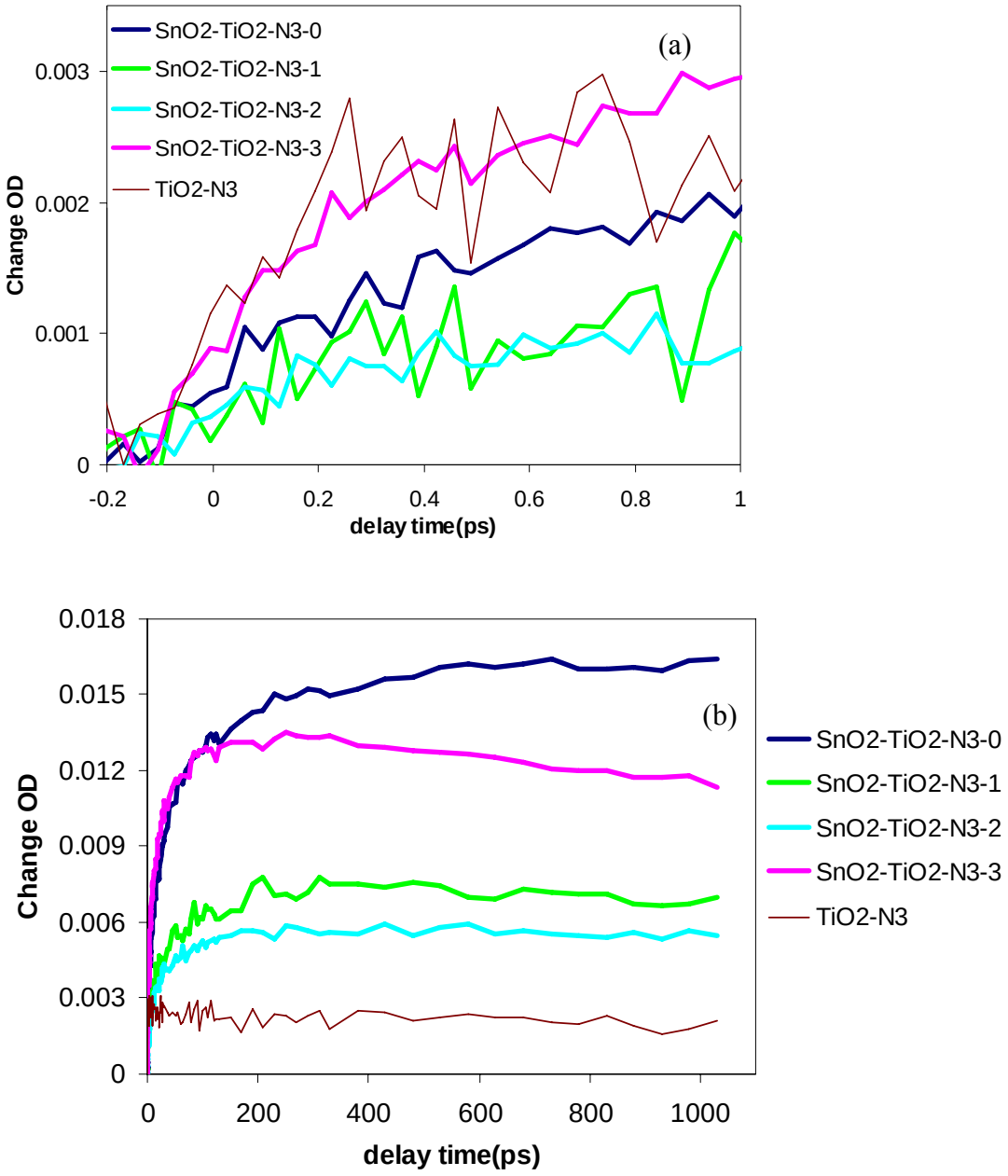

Figure 4.2 Comparison of the transient IR absorption signal for the RuN3- SnO_2 films with 0-3 insulating TiO_2 overlayers after correction of the absorption at 400nm to the same number of absorbed photons. (a) Shows the dynamics in the 1ns time scale. (b) Shows the dynamics in the 1 ps time scale.

From the OD corrected data in the 1ps time scale, we could tell N3 dye presents a faster electron injection to TiO_2 (blue curve) than that to SnO_2 (pink curve). Electron injection dynamics of SnO_2-N3 with 3 TiO_2 overlayers shows a similar fast component to that of TiO_2-N3, while Electron injection dynamics of SnO_2-N3 with 1 and 2 TiO_2 overlayers shows relatively slower component than SnO_2-N3 and TiO_2-N3. Because the extinction coefficient of electrons in SnO_2 is much larger than that of electrons in TiO_2 in our probing range, we expect the injection yield be decreasing with the increasing number of TiO_2 overlayers if electron injection from TiO_2 to SnO_2 happens. From the experiment, the injection yield decreases with the increase of number of TiO_2 overlayers from zero to two. However, the injection yield for that with 3 three overlayers is always larger.

Since all the dynamics are complete within the 1ns detection time window, we could compare the injection kinetics easily by normalizing them to the very end of delay time, Figure 4.3 Shows the comparison of the transient IR absorption signal for the RuN3-SnO_2 films with 0, 1, 2 and 3 insulating TiO_2 layers probed at 1905-2072 cm^{-1} normalized at the delay time of 1029 ps. It is shown that with the number of TiO_2 overlayer increasing, the dynamics of the electron injection become faster. It is probably because when the number of TiO_2 overlayer increases, the relative amount of TiO_2 within the system becomes larger, therefore the electron transfer component of N3-TiO_2 becomes apparent and closer to the dynamics of TiO_2-N3, which has the very fast component for the electron injection dynamics.

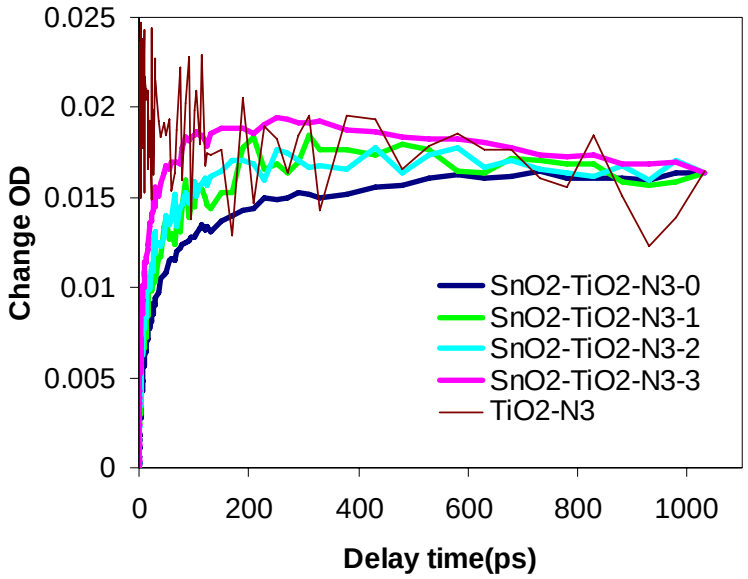

Figure 4.3 Comparison of the transient IR absorption signal for the RuN3- SnO_2 films with 0- 3 insulating TiO_2 layers normalized at the delay time of 1029 ps.

4.2 Ultrafast transient infrared spectroscopy of SnO_2-TiO_2 –C343

Electron injection dynamics from C343 to SnO_2 with 0, 1, 2 and 3 insulating TiO_2 overlayer were also monitored with transient mid-IR absorption measurement. C343 was first excited by 400nm pump beam, followed by electron injection into conduction band of SnO_2, where the injected electrons were probed with ranging from 1905 to 2072 wave numbers. Figure 4.4 shows UV-vis absorption spectra for the C343-SnO_2 films with 0-3 insulating TiO_2 overlayers. Figure 4.5 shows the electron injection dynamics which are scaled at pump position 400nm to the same absorbed photons.

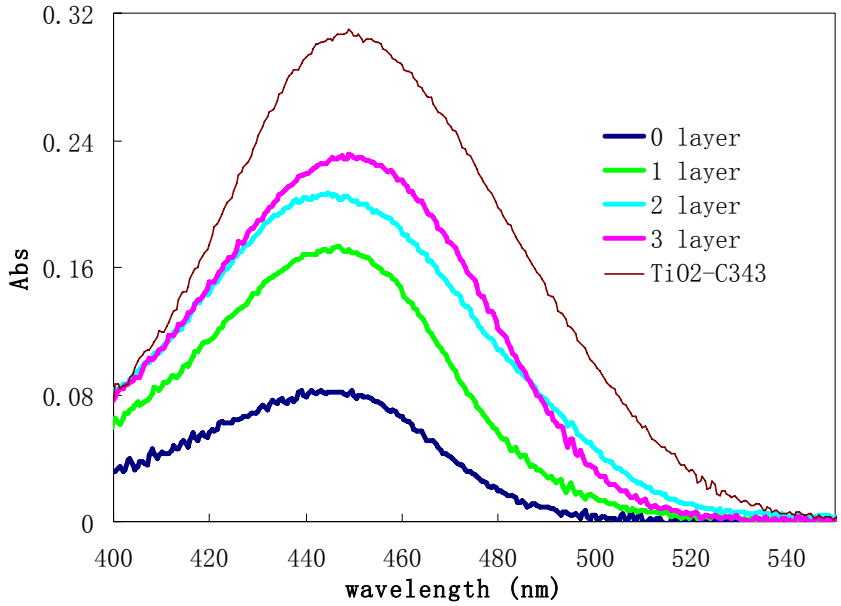

Figure 4.4 UV-vis absorption spectra for the C343-SnO_2 films with 0-3 insulating TiO_2 overlayers.

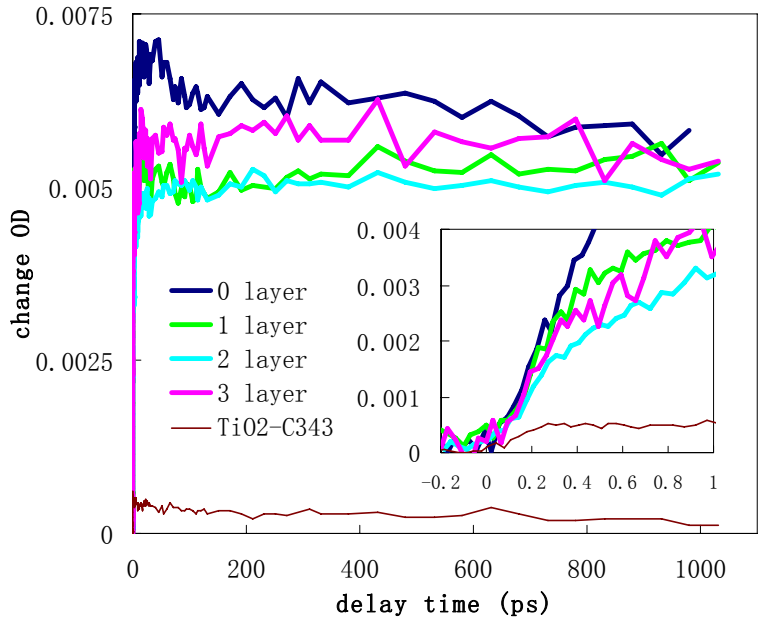

Figure 4.5 Comparison of the transient IR absorption signal for the C343- SnO_2 films with 0-3 insulating TiO_2 overlayers after correction of the absorption at 400nm to the

same number of absorbed photons. (a) Shows the dynamics in the 1ns time scale. (b) Shows the dynamics in the 1 ps time scale.

Since the signal for TiO_2-C343 is very small in the OD corrected dynamics, we can not take the dynamics of TiO_2-C343 into account when doing comparison. The injection yield decreases with the increase of number of TiO_2 overlayers from zero to two. However, the injection yield for that with 3 three overlayers is always larger.

If we just pick up the spectra of TiO_2-C343 and 0 layers, which is actually SnO_2-C343, we would observe that both of their dynamics possess a very fast signal increasing trend finished in several ps, and then followed by a gradual decreasing in the later delay time. However, if we focus on the dynamics of SnO_2-C343 with 1, 2, and 3 TiO_2 layer, we would clearly get that the signals of them did not decrease in the later delay time. Figure 4.6 shows the comparison of the transient IR absorption signal for the SnO_2-C343 films with 0, 1, 2 and 3 insulating TiO_2 overlayers after normalization to the same signal amplitude at 13ps where the signal size peak of SnO_2-C343 is. Compared with "0 layer", which is SnO_2-C343, we could see a clearly bigger signal size for "1 layer", "2 layers" and "3 layers" in the later delay time. Considering the signal comes from the electrons in the semiconductor and extinction coefficient of electrons in SnO_2 is much larger than that of electrons in TiO_2 in our probing range, the following three processes are considered to explain the signal size increase.

1) C343 $\rightarrow$ TiO_2; 2) C343 $\rightarrow$ SnO_2; 3) TiO_2 $\rightarrow$ SnO_2

We already know process 1) would be finished within 1ps and process 2) would be finished within about 13ps from the data. At this time, what is the cause of the increasing

signal of 1, 2 and 3 layer compared to 0 layers. We suspect the bigger signal comes from process 3) which is electron injection from TiO_2 to SnO_2. There might be other recombination processes in the system, but since they don't contribute to the signal increasing, they are not considered here.

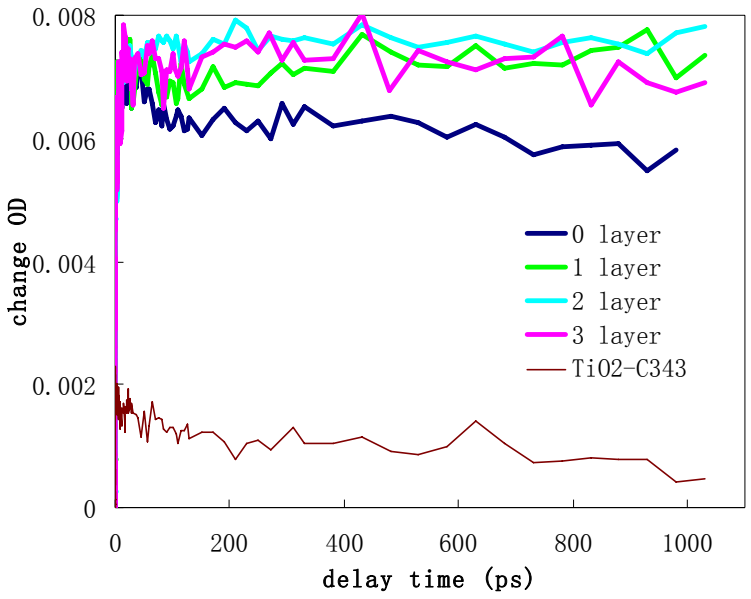

Figure 4.6 Comparison of the transient IR absorption signal for the C343-SnO_2 films with 0-3 insulating TiO_2 overlayers after normalization to the same signal amplitude at 13ps where the signal size peak of SnO_2-C343 is.

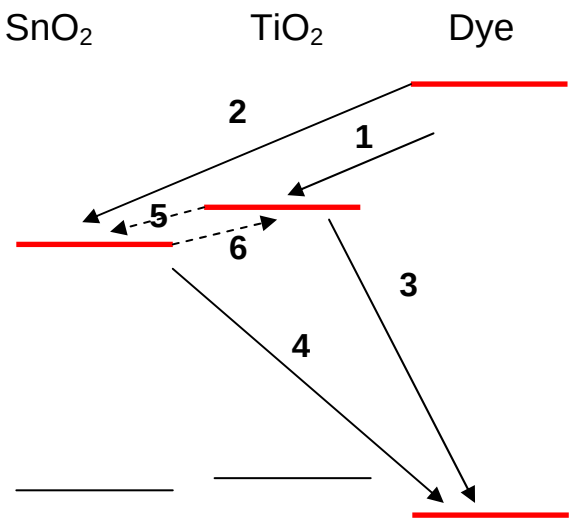

Figure 4.7 Electron transfer processes within SnO_2-TiO_2-Dye system

Figure 4.7 shows the main electron transfer processes within SnO_2-TiO_2-Dye system Within SnO_2-TiO_2-Dye system; we would mainly consider processes 1-6 which will contribute to our tested signal. From the kinetics of TiO_2-C343 and SnO_2-C343 shown in figure 4.6, we can say process 1,2,3,4 happened within our 1ns delay time scale. Yet this is a complex system because we have no idea if process 4 happened and also if it does happen, the time scale for process 5 is not clear, moreover, we do not even know if process 6 would happen since conduction bands of TiO_2 and SnO_2 are so close to each other.

4.3 Summary

The dependence of electron injection dynamics on the number of TiO_2 overlayers has been studied with ultrafast transient infrared spectroscopy in SnO_2-RuN3 and SnO_2-C343 systems. For the SnO_2-RuN3 system, electron injection dynamics become faster with the

increase of the number of TiO_2 overlayers. For both RuN3-TiO_2-SnO_2 and C343-TiO_2-SnO_2 systems, the injection yields decrease with the increase of number of TiO_2 overlayers from zero to two. However, the injection yields for that with 3 three overlayers is always larger. Detail is still to be understood.

Reference

[1] Chappel, S; Chen, S. G; Zaban, A. Langmuir 2002, 18, 3336-3342.

[2] O'Regan, B; Durrent, J. R; Sommeling, P.M; Bakker, N. J. J. Phys. Chem. C 2007, 111, 14001-14010.

[3] Kim, K; Benkstein, K. D; van de Lagemaat, J; Frank, A. J. Chem. Mater. 2002, 14, 1042-1047.

[4] Tirosh, S; Dittrich, T; Ofir, A; Grinis, L; Zaban, A. J Phys. Chem. B 2006, 110, 16165-16168.

Chapter 5 Interfacial Dynamic Study on the Film-based TiO_2-CdSe Nanocomposite

Quantum dot solar cells possess a promising future because of the Impact ionization effect which could reduce the thermalization loss by utilizing the excess energy of photogenerated carriers and promote greatly the quantum yield even upper than 1. A typical quantum dot solar cell includes a charge transport material attached on a quantum dot serving as light harvester. In this work TiO_2 is chosen as an electron transport material and several preparations of film-based TiO_2-CdSe nanocomposites qualified for the laser spectroscopy study are shown. Electron transfer dynamics from TOPO capped CdSe QDs to TiO_2 nanoparticles were investigated with both ultrafast transient absorption measurements and fluorescence lifetime measurements. Thiol and dithiocarbamate capped CdSe QDs were successfully prepared in an effort for the following preparing TiO_2-CdSe nanocomposite.

Quantum dot solar cell is a solar cell with quantum dots as light harvesting material and some charge transport materials, which are typically metal oxides, attached to the quantum dot to dissociate the excitons generated by photoexcitation of quantum dots followed by charge collection and conduction to produce electricity.

The reasons for quantum dots chosen as light harvesting material lies mainly in two aspects: 1. Tunable band edge of a quantum dot due to size quantization effect provide promising opportunities in harvesting the energy in visible solar spectrum. 2. Utilization of excess energy of hot carriers in quantum dots after photoexcitation offers an original

pathway to increase the photovoltage and photocurrent, which are two determinant parameters in a solar cell. Photocurrent in a quantum dot solar cell could be greatly enhanced due to the inverse Auger recombination or Impact ionization process of a quantum dot discovered and confirmed [2-5] by enormous reports from Nozik and Kilmov recently, which is actually a process to generate several excitons with one single photon by using the excess energy of photogenerated carriers to excite additional electron-hole pairs [6, 7]. With this process, thermalization (carrier cooling) problem, one of the four unavoidable losses in a solar cell paralleling incomplete absorption, recombination and thermodynamic loss, would be greatly ameliorated [8]. The quantum yield would exceed 1 if the process is active, which would theoretically enhance the photocurrent of a PV device greatly. On the other hand, photovoltage of a PV device could be enhanced with another form of utilization of the excess energy from hot carriers in which the carriers are extracted before they relax to the band edge via phonon emission, which require that the interfacial charge separation across the contacts to the semiconductor must be fast enough compared to the hot carrier cooling rate.

One of the important reasons for metal oxide material coming into consideration is the mesoporous film structure with high surface area of a metal oxide could provide a large folded support for the light harvesting material. Besides, some large-band-gap semiconductor metal oxides could accept electrons from electronically excited sensitizers, followed by electron percolation in the film with a fairly high diffusion coefficient (eg. 10^{-4} cm^2s^{-1} in TiO_2), therefore preparing metal oxide as a charge collector and conductor in the solar cell. Aparting from the reasons above, the stability of a metal oxide also make it favorable for solar cell electrodes.

As key processes within the operation of a solar cell, especially for quantum dot solar cell which is an excitonic PV device, charge separation and transfer along the interface between light harvesting materials and charge transport materials become extremely important since they would directly affect the photovoltage and photocurrent which are core parameters for a solar cell. The designing idea and development for a solar cell could be directed and benefit greatly from study of the interfacial dynamics. Even though much study on photovoltaic effect of a quantum dot solar cell with InP, CdS and CdSe etc. as photosensitizers has been investigated in the past decade, not much detailed interfacial dynamics were reported [9-12]. Recently Kamat [13] reported the interfacial dynamics between CdSe and TiO_2 nanocomposite in the colloid form showing a wide range of rate constant values between $7.3 * 10^9$ and $1.95 * 10^{11}$ S^{-1}, which provided detailed insight for charge separation even the system was not actually same as the real working electrode.

In our experiment, film based TiO_2-CdSe nanocomposite was chosen as a model which is more close to a real working PV device for the study of the interfacial dynamics within a solar cell. CdSe, as a typical quantum dot material, served as a light harvester while TiO_2 served as an electron transfer material to facilitate charge separation on the interface. In this experiment, electron transfer dynamics from TOPO capped CdSe QDs to TiO_2 nanoparticles were investigated with both ultrafast transient absorption measurements and fluorescence lifetime measurements. Thiol and dithiocarbamate capped CdSe QDs were successfully prepared in an effort for the following preparing TiO_2-CdSe nanocomposite.

Results and discussion

5.1 Photochemical stability of TiO_2-TOPO-CdSe nanocomposite

TiO_2-TOPO-CdSe nanocomposite system was prepared by immersing the metal oxide films directly into the CdSe QD solution to absorb CdSe particles followed by washing with the same CdSe QD solution solvent heptane.

The photochemical stability was still considered in this experiment. The nanocomposite sample was proved not stable in the condition of room light and air according to study on first exciton peak position absorption with UV-vis spectrophotometer. A clear blue shift of the first exciton peak position is shown from figure1; also we can observe an apparent decrease of the original absorption peak position.

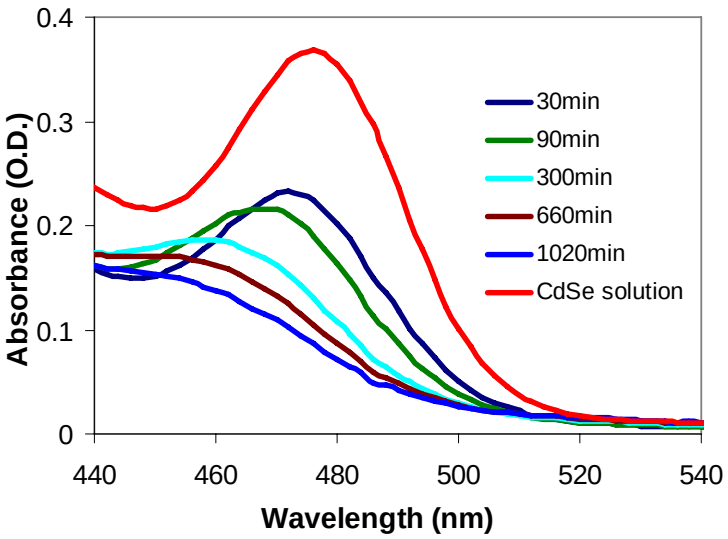

Figure 5.1. UV-vis spectra of TiO_2-CdSe sample of different time under room light and air

The reason for the instability of the sample was hypothesized that CdSe could be photoexcited by room light forming a fragile excited state sensitive to the oxygen and photo catalyst material TiO_2.

Similar photochemical stability tests of TiO2-CdSe samples under both conditions with room light blocked or air (oxygen) blocked by nitrogen purging were performed.

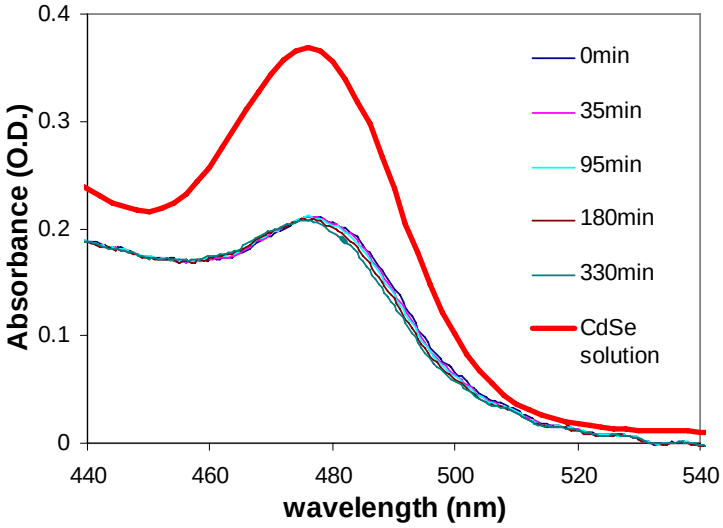

Figure 5.2 UV-vis spectra of TiO_2-CdSe sample with O_2 blocked

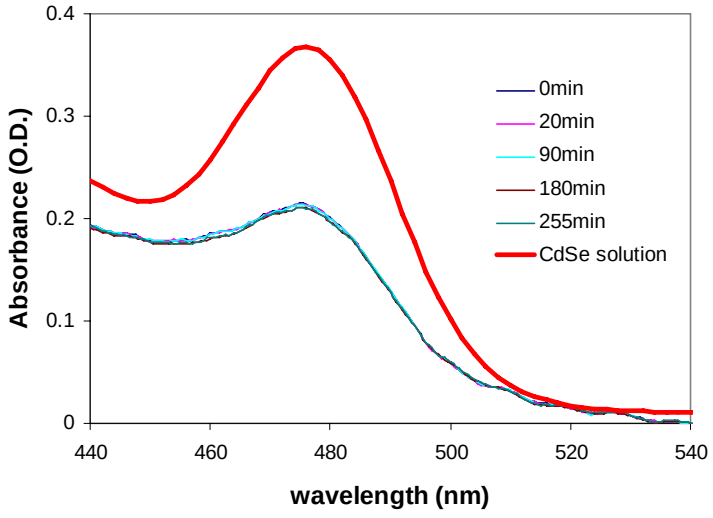

Figure 5.3 UV-vis spectra of TiO_2-CdSe sample with light blocked

This photochemical stability study suggests that the photo dependence of the CdSe- TiO2 nanocomposite sample requires by both light and oxygen, which directs us to just treat the sample with nitrogen purging to block the oxygen and therefore qualify the sample for the subsequent laser spectroscopy study.

5.2 Transient absorption dynamics for TiO_2-TOPO-CdSe nanocomposite

Information regarding electron transfer dynamics may be obtained with the pump-probe transient absorption measurements. In this experiment, transient absorption measurements in both visible and mid-IR spectral regions were performed attempting to analyze the electron transfer from photoexcited CdSe QDs to TiO_2 within the TiO_2-TOPO-CdSe nanocomposite system. ZrO_2-TOPO-CdSe nanocomposite system was chosen as a control because electron transfer from CdSe to ZrO_2 was supposed to be forbidden due to the far negative position of the conduction band of ZrO_2.

Several processes involving CdSe QDs could happen when CdSe QDs were excited in the CdSe-TOPO-metal oxide nanocomposite system.

$CdSe \xrightarrow{hv} h^+(CdSe) + e^-(CdSe)$ (1)

$e^-_{free}(CdSe) \longrightarrow e^-_{trap}(CdSe)$ (2)

$e^-_{trap}(CdSe) \longrightarrow e^-_{cb}(\text{metal oxide})$ (3)

$e^-(CdSe) + h^+(CdSe) \longrightarrow \Delta$ (4)

Quantum dots could be photoexcited to generate excitons followed by relaxation to conduction band edge through discrete quantized excited states before recombination. Oscillation strength of a transition to a certain quantized excited state would be decreased as a result of occupation of that corresponding state, which is known as state-filling.

Therefore, the bleach of transient absorption signal at a certain wavelength position could be an indication of the depopulation of that associated state after photoexcitation.

In our transient visible experiment, CdSe QDs with the particle size 2.1nm (first exciton peak 474nm) were first pumped at 470nm, which ensured electrons were nealy resonantly excited to the conduction edge allowing us to ignore intraband relaxation in CdSe QDs. The decrease of the ground state bleach after photoexcitation for the ZrO_2-TOPO-CdSe nanocomposite could be assigned to depopulation of ground state through recombination and trapping, while the decrease of the ground state bleach after photoexcitation for the TiO_2-TOPO-CdSe nanocomposite could be assigned to depopulation of ground state through recombination, trapping and electron transfer.

If an ideal and simple exponential kinetics model is applied to the depopulation of the ground state bleach in these metal-oxide-TOPO-CdSe systems, we could write

$N_t = N_0 e^{-k_i t}$ ZrO_2-TOPO-CdSe

$N_t = N_0 e^{-(k_i + k_{et}) t}$ TiO_2-TOPO-CdSe

Where K_i representing the decay rate constant contributed from trapping and recombination is the intrinsic decay rate constant for the ground state of CdSe; Ket is the electron-transfer rate constant; N_0 is the initial photoexcited electron population in the ground state of CdSe, N_t is the population in the ground state of CdSe at time t. The intrinsic decay rate constant K_i could be obtained from the dynamics of ZrO_2-TOPO-CdSe ground state bleach, while $K_i + K_{et}$ could be obtained from the dynamics of ZrO_2-TOPO-CdSe ground state bleach. Therefore, electron transfer rate information could be extracted out from this ideal model.

Transient visible absorption of both ZrO_2-TOPO-CdSe and TiO_2-TOPO-CdSe samples, clearly ground bleach recovery at 474nm were observed from both samples

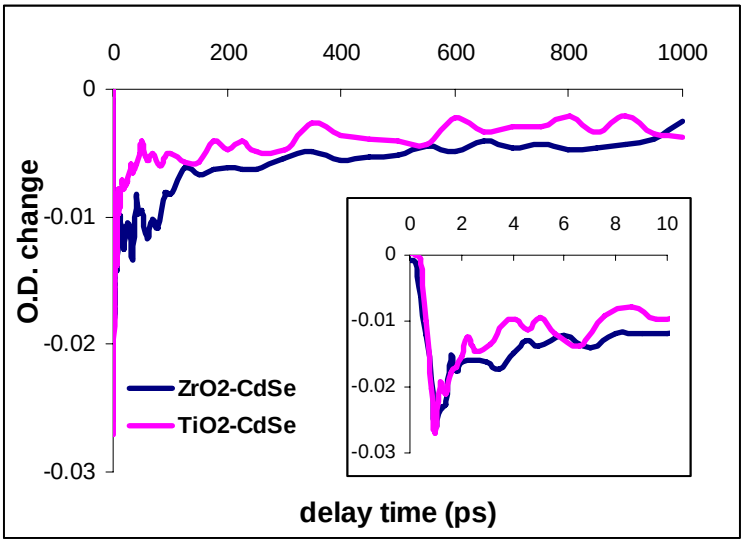

Figure 5.4 Comparison of ground state decay recovery between ZrO_2-CdSe and TiO_2-CdSe

Ground state decay dynamics of both metal-oxide-TOPO-CdSe systems were monitored with transient visible absorption spectroscopy. Similarity of the two ground state bleach dynamics with shows almost the unlikeliness of electron transfer from CdSe to TiO_2 in our TiO_2-TOPO-CdSe nanocomposite system.

To further analyze the electron transfer in our TiO_2-TOPO-CdSe nanocomposite system, Transient IR absorption experiment was performed. Both TiO_2-TOPO-CdSe and ZrO_2-TOPO-CdSe samples were first pumped at 480nm and probed in the mid-IR region. It is important to know that both intraband absorption of CdSe QDs and absorption from electrons in TiO_2 conduction band could contribute to the signal of our transient mid-IR absorption measurement. Light with 3200 wave number was chosen to probe the samples

since absorption cross section for CdSe intra band absorption is much bigger than that of electrons in TiO_2 conduction band, which allows us to ignore the absorption effect from TiO_2 conduction band, therefore facilitate our electron transfer study in this transient IR absorption experiment. For ZrO_2-TOPO-CdSe sample, since electron transfer is not assumed to happen, the transient IR signal is due to the depopulation of CdSe QDs excited state by trapping and recombination. For TiO_2-TOPO-CdSe sample, the decay of the signal is due to the depopulation of CdSe QDs excited state caused by trapping and recombination electron transfer from CdSe QDs to TiO_2 conduction band.

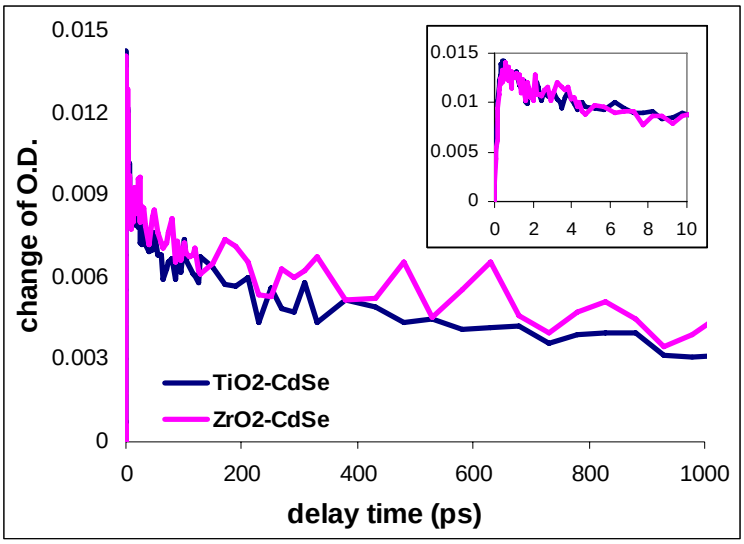

Figure 5.5 Comparison of transient mid-IR signal between ZrO_2-CdSe and TiO_2-CdSe

Dynamics of transient mid-IR signal of both metal-oxide-TOPO-CdSe systems were also monitored. The two dynamics with almost no difference shows no electron transfer was detected in our TiO_2-TOPO-CdSe nanocomposite system.

The reason for not observing electron transfer from CdSe to TiO_2 in our nanocomposite system is probably because the bridge between the two nanoparticles we used is so large

that the electron transfer would be significantly inhibited. With this consideration, further preparation of the CdSe- TiO_2 nanocomposite would concentrate on linking of TiO_2 and CdSe with shorter bridge molecules.

5.3 Fluorescence lifetime measurements for TiO_2-TOPO-CdSe

Fluorescence lifetime TiO_2-TOPO-CdSe sample was measured with the ZrO2-TOPO-CdSe sample was chosen as a comparison.

The rate r for the disappearance of excited state molecules is present by the following equation:

$$-d [A^*]/dt = (k_r + k_{nr}) [A^*] \ ; \qquad (5)$$

$$[A^*]_t = [A^*]_0 \exp(-t/r) \ ; \qquad (6)$$

$$r = 1/ (k_r + k_{nr}) \qquad (7)$$

k_r and k_{nr} are the rates for the radiative and non-radiative decay respectively. $[A^*]_t$ is the concentration of excited molecule at time t, while $[A^*]_0$ is the concentration of excited molecule at time zero. The fluorescence intensity is defined as the amount of photons emitted per unit time according to

$$A^* \rightarrow A + \text{photon} \qquad (8)$$

The fluorescence intensity i_F at time t after excitation by a short pulse of light at time zero is proportional, to the instantaneous concentration of molecules still at excited states $[A^*]_t$; the factor of the proportionality is the rate constant for radiative decay kr

$$i_F (t) = k_r [A^*]_t = k_r [A^*]_0 \exp(-t/r) \qquad (9)$$

If there is electron transfer within TiO_2-TOPO-CdSe nanocomposite system, the total disappearance rate for the excited state CdSe concentration after photoexcitation will

increase compared with the ZrO_2-TOPO-CdSe where electron transfer from CdSe to ZrO_2 is not supposed to happen since electron transfer as a contribution to the non-radiative decay of the CdSe excited state will increase the total decay rate of the excited state, therefore reducing the fluorescence intensity according to equation (9).

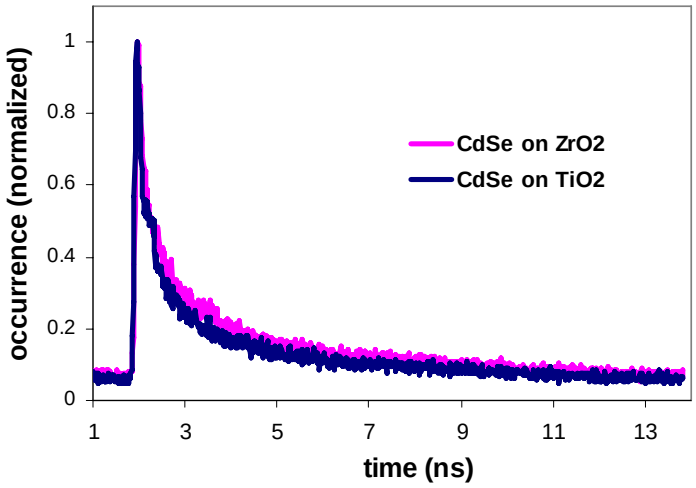

Figure 5.6 Comparison of fluorescence lifetime between ZrO_2-CdSe and TiO_2-CdSe

No apparent difference was observed from the comparison, which confirmed the unlikeliness for the electron transfer from CdSe to TiO_2. The long chain bridge molecule TOPO was considered as the limiting factor for the experiment. Based on this consideration, efforts in the following experiment were put to preparation of TiO_2-CdSe nanocomposite with shorter bridge molecules.

5.4 Preparation of TiO_2-CdSe nanocomposite with shorter bridge molecule

Two types of routes were designed to prepare the TiO_2-CdSe nanocomposite in our experiment. The original thought for our experiment is to use a bifunctional linker

molecule with carboxylate and thiol functional groups to linking TiO_2 film and CdSe QDs respectively.

1. The first trial for this bifunctional linker route in our experiment was to perform the ligand exchange process for the prepared TOPO-capped CdSe QDs, during which the bifunctional linker was attached onto CdSe QDs by replacing TOPO, followed by process in which TiO_2 film was immersed in the ligand-exchanged CdSe solution in an attempt to form the final TiO_2-CdSe nanocomposite.

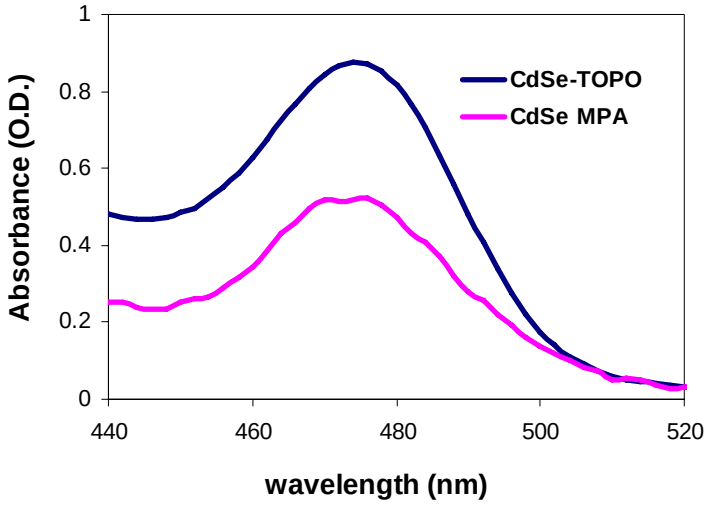

Figure 5.7 UV spectrums of CdSe-MPA and CdSe-TOPO

Mercaptopropionic acid (HOOC-CH_2-SH) was first tried in the quantum dot ligand exchanging process. The quantum dot CdSe after ligand exchange process was soluble in methonal and water, in which the TOPO capped CdSe can not be dissolved, which was an indication of the success of the ligand exchange. The first exciton peak position of the MPA capped CdSe did not change compared with the TOPO capped CdSe.

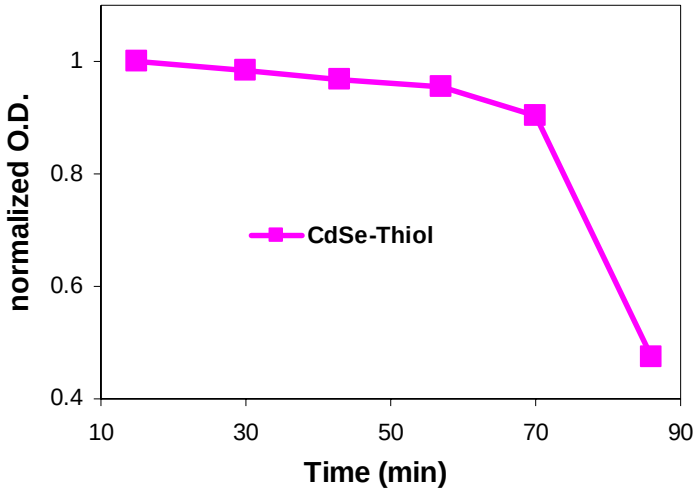

Figure 5.8 Temporal evolutions for the first exciton peak absorption of CdSe-Thiol

However, the temporal evolution of optical density at the exciton absorption peak shows that the stability of MPA capped CdSe quantum dot solution could not be maintained beyond 60 minutes, which made it unfavorable for our experiment.

2. These photochemical instability of thiol capped CdSe quantum dots motivated us to develop a new method for the ligand exchange of CdSe quantum dots.

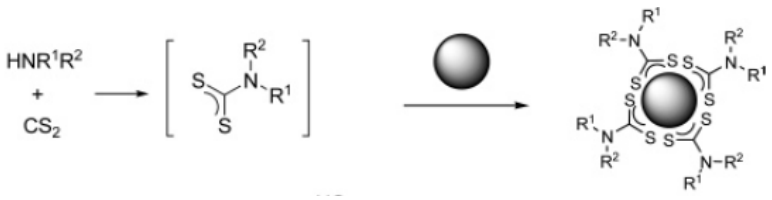

A bifunctional ligands, which contain a carbodithioate (-C(S)S-) function group was tried in the experiment. This type of molecule came into consideration because of their high affinity for metal atoms with the bidentate chelating binding of the carbodithioate group, which would increase the photochemical stability of the CdSe quantum dots after ligand

exchange. The ligand exchange process was performed according to the established literature.

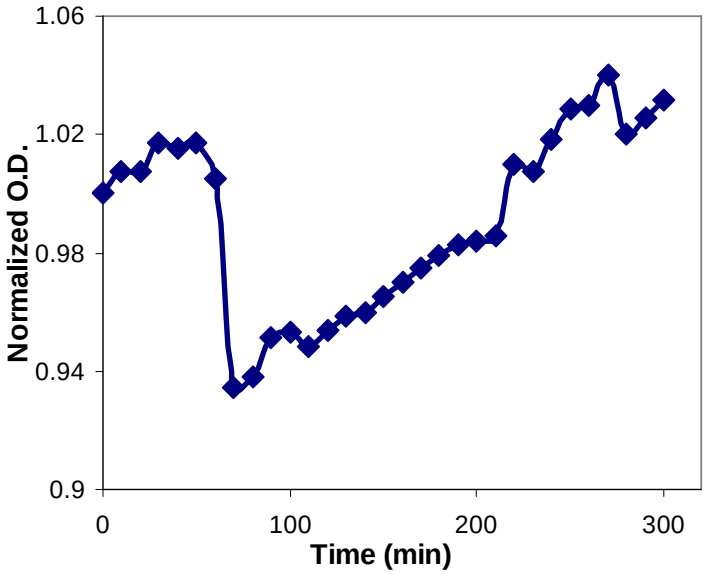

Figure 5.9 Temporal evolutions for the first exciton peak absorption of CdSe-carbodithioate

After the ligand exchange process, the quantum dot CdSe could be soluble in methonal and water, in which the TOPO capped CdSe can not be dissolved, which was an indication of the success of the ligand exchange. The temporal evolutions of the optical density at the first exciton peak position absorption were monitered by UV-vis spectrophotometer. Photochemical stability was significantly increased compare with thiol-capped CdSe quantum dots. Compared to the original optical density at the first exciton peak position, the absorbance was within 5% percent error even after 5 hours. However, unfortunately, this new ligand exchange route was proved still unfavorable because in the following TiO_2 film immersing process, the quantum dot could not attach onto the TiO_2 film surface.

5.5 Summary

Film based TiO_2-CdSe system was chosen as an object for laser spectroscopy investigating because of its significant position in the third generation solar cell. Electron transfer dynamics from TOPO capped CdSe QDs to TiO_2 nanoparticles were monitored with ultrafast transient mid-IR and visible absorption measurements. No electron transfer was observed from the analysis of both transient mid-IR and transient visible experiments probably because of the bridge material TOPO between CdSe and TiO_2 particles is too large to facilitate the electron transfer pathway. Based on the above assumption, several trials to prepare the TiO_2-CdSe nanocomposite with shorter bridge molecule were conducted. Thiol and dithiocarbamate capped CdSe QDs were successfully prepared in an effort for the following preparing TiO_2-CdSe nanocomposite with shorter bridge molecule. However, unfortunately, the ligand exchanged QDs were not favorable because of the photostability problem and little absorption onto TiO_2.

Reference

[1] M. A. Green, Prog. Photovoltaics 2001, 9, 123.

[2] Schaller, R. D.; Klimov, V. I. *Phys. Rev. Lett.* **2004**, *92*, 186601-186604.

[3] Schaller, R. D.; Sykora, M.; Pietryga, J. M.; Klimov, V. I. *Nano Lett.* **2006**, 6, 424-429.

[4] Shabaev, A.; Efros, A. L.; Nozik, A. J. *Nano Lett.* **2006**, 6, 2856-2863.

[5] Nozik, A. J. *Physica E* **2002**, *14*, 115-120.

[6] P.T. Landsberg, H. Nussbaumer, G. Willeke, J. Appl. Phys. 1993, 74, 1451.

[7] S. Kolodinski, J.H. Werner, T. Wittchen, H.J. Queisser, Appl. Phys. Lett. 1993, 63, 2405.

[8] M. C. Hanna and A. J. Nozika 2006 J Appl Phys, 100, 074510

[9] Zaban, A.; Micic, O. I.; Gregg, B. A.; Nozik, A. J, Langmuir; (Letter), 1998; 14(12); 3153-3156

[10] Vogel, R.; Weller, H. *J. Phys. Chem*. **1994**, *98*, 3183.

[11] Weller, H. *Ber. Bunsen-Ges. Phys. Chem.* **1991**, *95*, 1361.

[12] Hoyer, P.; Konenkamp, R. *Appl. Phys. Lett*. **1995**, *66*, 349.

[13] István Robel, Vaidyanathan Subramanian, Masaru Kuno, and Prashant V. Kamat J. 2006, Am. Chem. Soc., 128 (7), 2385 -2393.

[14] Aldana, J.; Wang, Y. A.; Peng, X, J. Am. Chem. Soc.; (Article); 2001; 123(36); 8844-8850.

[15] Fabien Dubois, Benoıˆt Mahler, Benoıˆt Dubertret, Eric Doris, and Charles Mioskowski, J. AM. CHEM. SOC. 2007, 129, 482-483

[16] Asbury, J. B.; Anderson, N. A.; Hao, E.; Lian, T. J. Phys. Chem. B 2003, 107, 7376.

[17] Guo, J.; Stockwell, D.; Ai, X.; She, C.; Anderson, N. A.; Lian, T. *J. Phys. Chem. B* 2006, 110, 5238.

[18] Ai, X.; Anderson, N. A.; Guo, J.; Lian, T. J. Phys. Chem. B 2005, 109, 7088.

[19] Ai, X.; Guo, J.; Anderson, N. A.; Lian, T. J. Phys. Chem. B 2004, 108, 12795.

[20] Guo, J.; She, C.; Lian, T. J. Phys. Chem. B. 2005, 109, 7095.